Construction and Building Materials 409 (2023) 133828

Contents lists available at ScienceDirect

Construction and Building Materials

journal homepage: www.elsevier.com/locate/conbuildmat

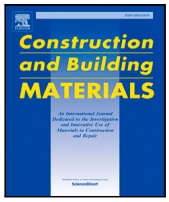

Water diffusion mechanisms in bitumen studied through molecular dynamics simulations

Lili Ma [a], Hirad S. Salehi [b], Ruxin Jing [a], Sandra Erkens [a], Thijs J.H. Vlugt [b], Othonas A. Moultos [b,*], Michael L. Greenfield [c], Aikaterini Varveri [a]

[a] Department of Engineering Structures, Faculty of Civil Engineering and Geosciences, Delft University of Technology, Delft, Netherlands
[b] Engineering Thermodynamics, Process & Energy Department, Faculty of Mechanical, Maritime and Materials Engineering, Delft University of Technology, Delft, Netherlands
[c] Department of Chemical Engineering, University of Rhode Island, Kingston, RI, United States

ARTICLE INFO

Keywords:
Bitumen
Water diffusion
Water cluster
Molecular dynamics
Phase separation
Hydrogen bonding

ABSTRACT

Water transport is one of the major factors responsible for moisture damage in asphalt pavements. To study the thermodynamics and kinetics of water transport in bitumen and to uncover microscale mechanisms of moisture-induced damage, molecular dynamics simulations were performed for up to 600 ns for water–bitumen systems with realistic water contents that varied from 0 to 1.76 wt%. Hydrogen bonding interactions and clustering of water molecules at various combinations of temperature and water content were investigated, and their effects on the self-diffusion coefficient of water and bitumen properties are computed and discussed. It is shown that the saturated water concentration in bitumen is small, especially at low temperatures, and additional water molecules tend to form large water clusters via hydrogen bonding, indicating micro-phase separation of the water and bitumen phases inside the simulation box. Hydrogen bonding and water clustering play a crucial role on the magnitude of the self-diffusion coefficient of water. Physical properties of bitumen that include viscosity and cohesive energy are affected by water. The presence of large water clusters is indicative of how degradation in cohesion is observed on the microscale.

1. Introduction

Bitumen is a highly viscous residue of crude oil distillation [1] that is commonly processed for use in roadway construction. After further processing, bitumen is also used in roofing, dike protection, and sealing of engineering structures [2]. In pavement engineering, bitumen is an essential element of an asphalt mixture. In combination with additives and mineral fillers such as sand, it functions as the mastic that binds mineral aggregates.

The presence of water, either as a vapor or a liquid, has been considered as one of the main causes of various pavement distresses such as raveling, stripping, and cracking [3,4]. The fundamental mechanisms behind these distresses, collectively called moisture damage in the literature, are cohesive and adhesive degradation [3]. Moisture in voids within asphalt pavement initially diffuses into bitumen, resulting in cohesive degradation of bitumen and mastic, and then reaches the mastic-aggregate interface, where it leads to a loss of adhesion [5]. A distinction is assigned between cohesive failure and adhesive failure on a basis of macroscopic observations of the failure location.

Research has been conducted to compare the relative importance of adhesive and cohesive failures in moisture damage. It has been reported that the decrease in adhesive strength is larger than the decrease in cohesive strength as the exposure time to moisture increases. This indicates a change in failure mode from cohesive failure at dry conditions to adhesive failure at wet conditions [6,7], and it suggests that adhesive failure is a more important contributor to moisture damage compared with cohesive failure. Cohesion is shown to contribute to moisture damage mainly by controlling the rate of moisture diffusion and the subsequent absorption of moisture through mastic and into the mastic-aggregate interface [8]. Some prior studies, however, state that cohesive failure is a more common mode of moisture damage [9,10]. For a more comprehensive description of moisture damage and its relationship to bitumen, the reader is referred to additional review papers [11,12]. Overall, moisture can soften bitumen and mastic and can weaken the cohesive forces between them. This process is attributed to moisture saturation [13,14], but the extent that cohesion can be affected by moisture is not certain yet. The mechanism of how moisture saturation decreases cohesion is not experimentally validated.

* Corresponding author.
E-mail addresses: O.Moultos@tudelft.nl (O.A. Moultos), greenfield@uri.edu (M.L. Greenfield).

https://doi.org/10.1016/j.conbuildmat.2023.133828
Received 28 June 2023; Received in revised form 11 October 2023; Accepted 13 October 2023
Available online 24 October 2023

The chemical composition of bitumen influences its physical and chemical properties [15]. Bitumen composition further affects the solubility and diffusion coefficient of absorbed water [8]. Bitumen is not a single, well-defined material. Instead, the term refers collectively to similar materials whose chemical compositions depend on crude oil source, additives, processing steps, and aging. The chemical components that comprise a bitumen of interest can be classified on a basis of solubility into saturates, aromatics, resins, and asphaltenes, typically known as SARA fractions [1]. The saturates fraction in bitumen consists of nonpolar aliphatic hydrocarbons. Aromatics (sometimes called naphthene aromatics) comprise hydrocarbons with saturated and aromatic rings. Resins (sometimes called polar aromatics) and asphaltenes contain functional groups with heteroatoms (nitrogen, sulfur, and oxygen), which strongly influence the physicochemical properties of bitumen [16]. Asphaltenes are distinguished from the other fractions by insolubility in a nonpolar solvent, such as *n*-heptane. Saturates, aromatics, and resins are sometimes collectively referred to as maltenes.

The predominantly hydrophobic composition of bitumen leads to it having a low absorption capacity for water [8,17,18]. Various maximum water absorption data in bitumen have been measured. They span from ca. 0.5 wt% after 4 days (bitumen in contact with air at 80% relative humidity) [18] to 7 wt% (bitumen immersed in water for 10.75 days) [19] to 2.5 wt% (bitumen immersed in water) yet still rising after hundreds of days [17]. Differences that arise solely from the phase of water (liquid or vapor) indicate non-thermodynamic factors that influence its absorption. Because liquid water and saturated water vapor have the same chemical potential at equilibrium, the absorbed amount of water would be the same if water chemical potential was the only driving force of absorption and if all water was molecularly dispersed in bitumen. Factors that arise from mass transfer limitations, such as fluid flow through pores in an asphalt mixture, could contribute to these differences. Water absorption and diffusion in mastic have also been shown to depend on the types of filler and fine aggregate [20]. Further, water absorbed in bitumen is assumed to occupy distinct states. Some water is assumed to absorb to polar functional groups [17,19], while the remainder forms water clusters [18]. Nano-scale water phases would not face a maximum in water content if they could continue to grow in size. Both water absorption and water clustering significantly decrease the diffusion coefficient of moisture in bitumen. Distinguishing among all these effects is important in order to understand the potential for moisture damage in a pavement over relevant real-world length and time scales.

Several experimental techniques can quantify the moisture absorption and transport rate in bitumen. Gravimetric methods measure the change in moisture absorption with time [8,17,18]. Spectroscopic methods (such as infrared and electrochemical impedance spectroscopy) identify changes in water concentration [21–23]. Each method invokes different assumptions that can affect the magnitude of the diffusion coefficient that is obtained for water in bitumen.

Various diffusion models have been used to interpret experimental measurements. It has been shown that models based on a constant diffusion coefficient in Fick's law fail to describe moisture diffusion in bitumen properly [21]. The dual model [21], the Langmuir-diffusion model [22], the diffusion-reaction model [17], and the cluster model [18] have been proposed as alternatives. These models assume that water molecules in bitumen are present in two modes: a free mode and a bound mode. The free mode refers to water molecules that freely diffuse in bitumen, while the bound mode assumes that water is confined to polar bitumen sites due to hydrogen bonding [21]. These alternatives differ in the diffusion dynamics of the bound mode. In the dual model, the diffusion coefficient of bound water is significantly lower than that of free water, indicating partial immobility. Meanwhile, the Langmuir, reaction, and cluster models classify bound water as completely immobile.

The overall hydrophobicity of bitumen, the polarity of its functional groups, and the polarity of water make the interactions between moisture and bitumen rather complex. When different diffusion models are applied to results from different experimental techniques, water diffusion coefficients are calculated that span from 10^{-17} to 10^{-9} m^2/s [24]. The lower range of diffusivities is usually obtained from spectroscopic measurements, in which water-related peak areas are integrated in order to estimate concentration variations through time. The faster dynamics are typically obtained using the gravimetric technique (mass uptake) [12]. In addition, bitumens that are derived from different crude oil origins also exhibit different water absorption and diffusivity [8,25,26].

The discrepancies among different measurements make it difficult to quantify a single diffusion coefficient of moisture in bitumen [18] and to conclude an exact diffusion mechanism. To this end, molecular simulations have the potential to provide useful insight into the underlying mechanisms and to explain why discrepancies in measurements of water diffusion rates occur. In the past two decades, molecular simulation has been used for complementing and interpreting experimental measurements of the physicochemical, structural, and dynamic properties of bitumen. A prerequisite for accurate molecular simulations of bitumen is a well-defined model that represents the chemical composition and physicochemical properties of bitumen [27,28]. Early models [29] represented bitumens from different crude oil sources by proposing a different "average" molecule to represent the diversity of functional groups in each bitumen. Such a representation cannot exhibit the well-known separation of bitumen into solubility-based SARA fractions, as described in an earlier review [30]. The three-component models developed by Zhang and Greenfield [31] (ZG07) represented most solubility classes, yet molecular weights of maltenes were too small, and several polar group functionalities were lacking. A six-component model proposed by Zhang and Greenfield [32] included those functionalities, yet most molecules were still too small. The four molecule types in the Cooee model created by Hansen et al. [33] used molecule size and shape to distinguish among separate solubility classes; all molecules lacked partial charges. Their use of a united atom model further sped up the computation rate. The twelve-component systems proposed by Li and Greenfield [27] (LG14) made better representations of the polarity and molecular weights of each SARA fraction that were aided in part by choosing molecular structures that had been identified by others in geochemistry studies. Many groups have now employed the composition proposed by Li and Greenfield to represent bitumen AAA-1 of the Strategic Highway Research Program [34] in molecular simulations. The LG14 composition has been modified by many researchers in order to use either fewer molecule types or a greater range of molecule sizes and functionalities, as documented in a recent review [35].

Molecular dynamics (MD) simulations have been previously performed to gain insights into the mechanisms of water diffusion in bitumen. Lemarchand et al. [28] conducted MD simulations of 43 ns duration using the Cooee model with additions of 0.06–4 wt% water and partial charges at sulfur sites in the bitumen. At 377 K and 452 K and almost all concentrations, most water molecules formed a single large droplet. At 377 K, trends over the final 14 ns suggested that water molecules would form a single droplet after a sufficiently long simulation. Analysis of water mean-squared displacement (MSD) over long times showed a decrease in the diffusion rate with increasing water content. This was caused by the formation of water droplets. Radial distribution functions (RDFs) indicated that these droplets were usually located near saturate chain molecules. The cohesive energy density (CED) of the system decreased with increasing water content due to the volume increase exceeding an increase in water interactions [28]. Xu and Wang [36] studied a bitumen-aggregate system with 7–14 wt% water added to the interface. They sampled interface fluctuations in MD runs of 0.05 ns and found that water molecules

at the interface between ZG07 bitumen and a silica or calcite aggregate surface weakened the adsorption of bitumen and decreased the thermodynamic work of adhesion. This resulted in a change that can be interpreted on the macroscopic scale as moisture-induced damage. This was also observed by Liu et al. [37], who explained that adhesive failure resulted from the replacement of bitumen–aggregate hydrogen bonds with water–aggregate hydrogen bonds. Du et al. [38] performed MD simulations of bitumen–water systems using the LG14 model for 1 ns per simulation condition. The water concentrations considered were in the range 1 – 20 wt%. In this study, too, large water clusters formed at most concentrations. The authors reported an increase in the overall water diffusivity in bitumen, which is contrary to experimental observations [18] of a decrease in diffusivity with increasing water content. For extensive lists of studies, the reader is referred to a recent review [39].

The vast majority of prior MD simulation studies of water in bitumen have been performed using conditions that fail to achieve a sufficient description of water diffusion as it arises in real-world systems. The main source of this failure is the short sampling time, which is usually limited to a few hundred ps up to 1 ns. Such short MD simulations do not allow for the proper equilibration of the highly viscous bitumen structure, even at elevated temperatures. Although averaged quantities such as density may appear constant with sampling time, this can arise because they have not yet begun to fluctuate significantly, rather than that they have fully converged. Similarly, the short sampling times used for water diffusivity in bitumen in most MD studies do not ensure that proper diffusion behavior (converging to the actual diffusive regime [40] in which mean-squared displacement increases linearly in time) is achieved. These issues are particularly pronounced in simulations at lower temperatures, i.e., close to ambient or colder. Apart from the short runs, some prior simulation studies have considered water concentrations that are much larger than those observed experimentally [8,19]. Simulations at smaller water concentrations are required for explaining moisture diffusion behavior that is observed in experiments, which are necessarily below the solubility limit. Simulations of bitumen that probe long time scales [28,41] reveal effects with much longer relaxation times than can be quantified in simulations of only 0.1 to 1 ns.

In this work, we primarily aim to provide useful insights into water transport mechanisms in bitumen by means of molecular dynamics simulations. We also aim at performing simulations over time and length scales beyond those of current common practice to ensure reliable and accurate predictions. To mitigate the common simulation drawbacks discussed earlier, we perform MD simulations of water–bitumen using the LG14 model bitumen system and water concentrations closer to levels observed in experiments. To overcome equilibration and convergence problems, we perform simulations of up to 600 ns (0.6 μs), which are orders of magnitude longer than most of the available studies to date. To investigate water diffusion mechanisms, we study hydrogen bonding and water clustering in the water–bitumen systems. At water concentrations that are low but not the lowest simulated here, formation of large water droplets (i.e., water clusters via hydrogen bonding) is observed due to micro-phase separation. RDFs of water molecules and bitumen components reveal the close proximity of water droplets to heteroatoms in bitumen. Due to this network, a sharp decrease in the self-diffusion coefficient of water with increasing water content is observed. The presence of water also decreases the viscosity and cohesion of bitumen. We expect that our results can provide a micro-scale comparison among diffusion models and a guideline on the meanings of diffusion coefficients at different orders of magnitude.

This paper is organized as follows. Section 2 contains the force field and simulation details of the water–bitumen systems. In Section 3, the simulation results are presented. The formation of water clusters is quantified, which guides subsequent discussion of structural and physicochemical properties of water–bitumen systems, including density, viscosity, and cohesive energy. In Section 4, a comparison is made between the simulation results and the assumptions that are invoked within macro-scale water diffusion models. The main conclusions are summarized in Section 5.

2. Methods

2.1. Force field parameters

The Optimized Potential for Liquid Simulations All-Atom (OPLS-AA) force field [42,43] was used to model bitumen. The force field parameters were obtained from the work of Li and Greenfield [27], who supplemented the OPLS-AA implementation available in Towhee software [44] with additional parameters to address molecular architectures that were missing in prior parameterizations. OPLS-AA has been shown [27,31] to be successful enough in modeling bituminous materials, for which it is impossible to make a one-to-one connection between experimental data and molecular composition on a molecule-by-molecule basis. The OPLS-AA force field considers the contributions of bonded terms, i.e., bond stretching, angle bending, backbone torsion, and improper torsion to maintain planarity [45], and non-bonded terms, i.e., Lennard-Jones (LJ) and Coulombic interactions. A cutoff of 10 Å was used for the LJ interactions. Analytic tail corrections of long-range van der Waals forces were used for energy and pressure. The long-range electrostatic interactions beyond 10 Å were computed via the Particle-Particle Particle-Mesh (PPPM) method with a relative precision of 10^{-5} [46]. Geometric combining rules were used for the LJ interactions between non-identical atoms, as implemented into OPLS-AA development and parameterization [42]. A scaling factor of 0.5 was used for all interactions between atom pairs separated by 3 bonds [42]. The extended simple point-charge (SPC/E) model [47] was used for water. SPC/E is a rigid three-site water model that shows good agreement with experimentally measured transport [48,49], thermodynamic [50], and structural [51] properties of pure water. Hydrogen bonding arises through favorable Lennard-Jones and Coulombic interactions. The RATTLE extension [52] of the SHAKE algorithm [53] was used to fix the bond lengths and bond angle of each water molecule. All force field parameters are listed in Tables S1 – S6 in the Supplementary Material.

2.2. Composition and simulation details

The 12-component all-atom LG14 model [27] was used to represent the saturate, aromatic, resin, and asphaltene fractions in bitumen. Its composition was devised to represent the AAA-1 bitumen of the Strategic Highway Research Program (SHRP) [54]. The exact components comprising LG14 are shown in Fig. 1. As noted in Fig. 1, functional groups that contain heteroatoms (sulfur, nitrogen, and oxygen) are present in all five polar aromatics (quinolinohopane, thio-isorenieratane, benzobisbenzothiophene, pyridinohopane, and trimethylbenzene-oxane) and in all three asphaltenes (asphaltene-phenol, asphaltene-pyrrole, and asphaltene-thiophene). Details of the molecular architectures, assignments of atom types for the 12 molecule types, and overall composition of the model bitumen are provided in Figs. S1–S9 and Table S7.

In the MD simulations, 72 molecules (containing 5572 atoms) were used for the bitumen phase (following the mole fractions of the LG14 AAA-1 model). Subsequently, 0, 2, 4, 8, 16, or 32 water molecules were added. These system sizes correspond to water concentrations in bitumen on the macroscale of 0 wt%, 0.11 wt%, 0.22 wt%, 0.44 wt%, 0.93 wt%, and 1.76 wt%, respectively. The simulations do not incorporate water present in microvoids, filler, or aggregate particles because the focus here is on bitumen, and those components of an asphalt mixture arise over much larger length scales. All simulations here were performed at a pressure of 1 atm to mimic atmospheric conditions. Higher pressures can increase the density of bitumen slightly and can impact transport properties such as the viscosity of bitumen and the self-diffusion coefficient of water in bitumen. Such an investigation is outside the scope of this work.

Simulations were performed at six temperatures, i.e., 298.15 K, 313.15 K, 353.15 K, 393.15 K, 443.15 K, and 533.15 K. This temperature range spans ambient temperature (often encountered in pavement

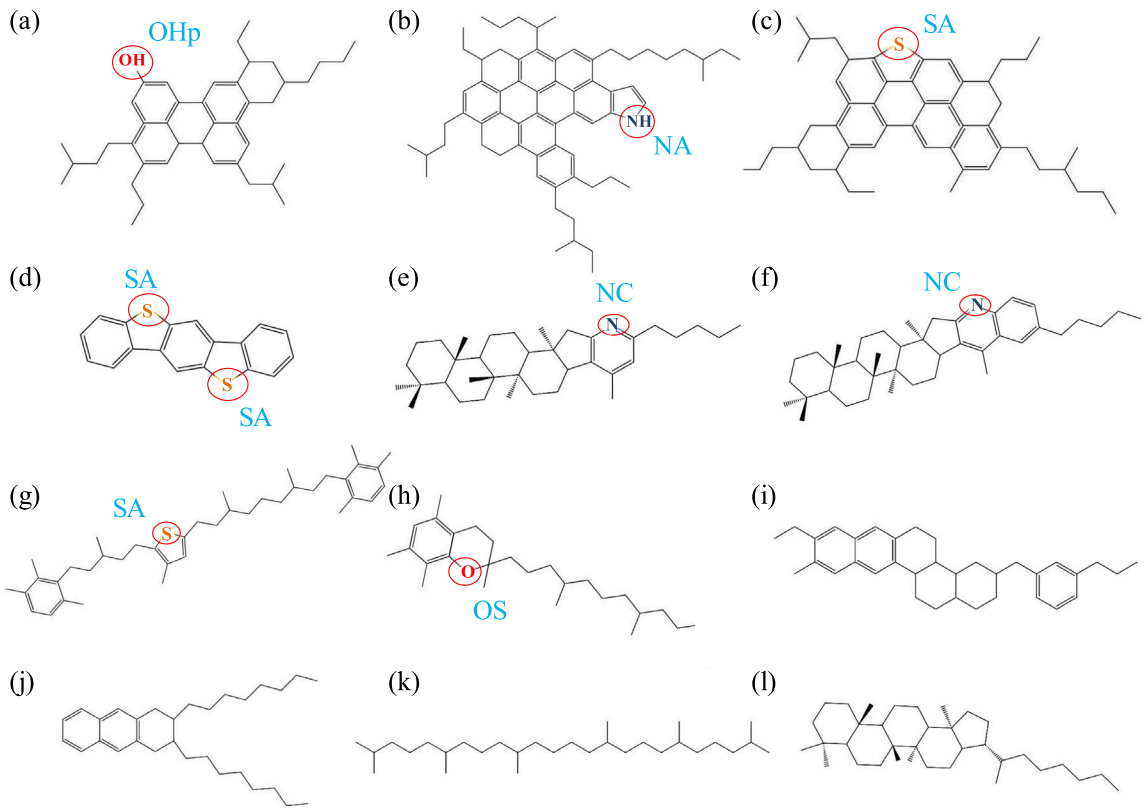

Fig. 1. Chemical components that comprise the LG14 bitumen model [27]. Asphaltene molecules: (a) asphaltene-phenol, (b) asphaltene-pyrrole, and (c) asphaltene-thiophene; resin molecules: (d) benzobisbenzothiophene, (e) pyridinohopane, (f) quinolinohopane, (g) thio-isorenieratane, and (h) trimethylbenzene-oxane; aromatic molecules: (i) perhydrophenanthrene-naphthalene (PHPN) and (j) dioctyl-cyclohexane-naphthalene (DOCHN); saturate molecules: (k) squalane and (l) hopane. Red circles indicate heteroatom-based functional groups; their OPLS-aa atom types are denoted by blue labels. (For interpretation of the references to color in this figure legend, the reader is referred to the web version of this article.)

applications), medium-high temperatures (i.e., 313 K and 353 K) that are the upper limit for experimental measurements of water diffusion behavior [18], and very high temperatures (i.e., 443 K and 533 K). Although the high temperatures considered here are not typically observed during the service life or processing of bitumen or of asphalt mixtures, they allow for reaching relatively well-equilibrated configurations without requiring prohibitively long MD simulations, while still being able to provide important physical insight into water transport behavior in bitumen. This is because the physical mechanisms that govern water diffusion in bitumen are fundamentally similar at both low and high temperatures. Performing MD simulations at high temperatures is common practice in molecular simulation studies of bitumen [28,41,55]. Our simulation results at 533 K can be directly compared to results from these previous studies.

All MD simulations were performed using the open-source LAMMPS software (version 22 August 2018) [56,57] according to the following procedure. Initial configurations of one water–bitumen system per composition were generated in Packmol [58]. Energy minimization of each system was performed using the conjugate gradient algorithm. Periodic boundary conditions were applied in all directions. To create independent configurations, an *NPT* simulation was performed at 1000 K and 1 atm for 5 ns with a time step of 1.0 fs. Configurations were obtained from the simulation trajectories at 1.0 ns, 2.0 ns, 3.0 ns, 4.0 ns, and 5.0 ns. Next, each of these five water–bitumen systems were quenched to each temperature of interest and were equilibrated in the *NPT* ensemble at 1 atm to ensure that density and total energy converged to stable fluctuations. The Nosé–Hoover thermostat and barostat with coupling constants of 100 and 1000 fs, respectively, were used to regulate the temperature and pressure [59]. Then, equilibration runs in the *NVT* ensemble were carried out in a simulation box whose volume was set equal to the average volume computed from the *NPT* runs in the previous step. Finally, production runs in the *NVT* ensemble were performed to compute transport and structural properties of the water–bitumen systems. The durations of the production runs were determined from the time needed for the transport properties (self-diffusion coefficient and viscosity) to converge. These were indicated by linear increases with time of the mean-squared displacement and the mean-squared stress fluctuations [40]. The durations of all equilibration and production simulations for the systems studied here are listed in Table S8. The positions of atoms were recorded every 10 ps for the simulations at 533.15 K and every 100 ps for the simulations at all other temperatures. Averages and standard deviations of all simulation results were obtained from five independent runs at each composition.

2.3. Hydrogen bonding and water clusters

Hydrogen bonding and clustering of water molecules were quantified to study the mechanism of water diffusivity in bitumen. Hydrogen bonds were detected based on two criteria: (1) the distance between a hydrogen bond acceptor and a hydrogen bond donor is less than 3.5 Å, and (2) the angle between a hydrogen atom, a hydrogen bond donor, and a hydrogen bond acceptor is less than 30° [60]. Potential acceptors were considered to be the oxygen atom of water and the heteroatoms of bitumen that are circled in Fig. 1. Potential donors are the oxygen of water and the bitumen heteroatoms OHp and NA that are bonded to hydrogen.

Neighboring water molecules were considered to be in a cluster when their oxygen atoms were within the hydrogen bonding distance of 3.5 Å. Water clusters were identified by using the clustering algorithm of Sevick et al. [61]: in a system with N water molecules, first all water–water distances (i.e., oxygen-oxygen) are computed. An $N \times N$ symmetric water pair matrix $\boldsymbol{C}$ is then generated, where C_{ij} equals 1

if the distance between water molecules i and j is smaller than 3.5 Å (the molecules i and j are referred to as directly connected pairs) or C_{ij} equals 0 otherwise. The next step is to find water molecules that are indirectly connected. If $C_{ij} = 1$ and $C_{jk} = 1$, then water molecules i and k are also connected, i.e., $C_{ik} = 1$, thus forming a cluster assembly composed of water molecules i, j, and k. To this purpose, one water pair with $C_{\ell m} = 1$ is randomly selected as an initial cluster assembly. All other water pairs with $C_{ij} = 1$ are considered, and the water molecules in these pairs are ascribed to this assembly when these pairs have common water molecules (i or j equals ℓ or m). The process is repeated until no more additions are found, and the total number of water molecules in this assembly is denoted as the cluster size. Then, a new indirect search is repeated by starting with a remaining water pair (not in this cluster) identified as a new initial cluster assembly. These steps are executed repeatedly until all cluster assemblies are identified.

RDFs were also computed to analyze the positions of hydrogen bonds and water clusters in bitumen. An RDF describes the average distribution of particles around a central reference particle. RDFs were sampled up to a distance of 25 Å with 100 bins by using the LAMMPS `rerun` command.

2.4. Transport properties and cohesive energy

The OCTP plugin [40] in LAMMPS was used for an on-the-fly calculation of the shear viscosity,

$$\eta = \lim_{t\to\infty} \frac{1}{10\cdot 2t}\frac{V}{k_B T}\left\langle \sum_{\alpha\beta}\left(\int_0^t P^{os}_{\alpha\beta}(t')\,dt'\right)^2\right\rangle \tag{1}$$

where

$$P^{os}_{\alpha\beta} = \frac{P_{\alpha\beta}+P_{\beta\alpha}}{2} - \delta_{\alpha\beta}\left(\frac{1}{3}\sum_{k=x,y,z} P_{kk}\right) \tag{2}$$

V is the volume of the system, $P^{os}_{\alpha\beta}$ are the traceless and symmetric pressure tensor components, t is the correlation time, k_B is the Boltzmann constant, T is the absolute temperature, and $\delta_{\alpha\beta}$ is the Kronecker delta. The angle brackets $\langle\ \rangle$ denote an ensemble average. The computation of η in MD does not depend on the system size [62–64].

The self-diffusion coefficient of water was computed using the OCTP plugin [40] according to

$$D_{self} = \lim_{t\to\infty}\frac{1}{6tN_w}\left\langle \sum_{i=1}^{N_w}\left(\boldsymbol{r}_i(t)-\boldsymbol{r}_i(0)\right)^2\right\rangle \tag{3}$$

where N_w is the number of water molecules, $\boldsymbol{r}_i$ is the position vector of the ith water molecule, and the averaged summation provides the MSD. Self-diffusion coefficient has been shown to depend on the system size [65,66]. To correct diffusivity for finite-size effects, the Yeh–Hummer (YH) correction term was used [62,65–67]:

$$D^{\infty}_{self} = D_{self} + \frac{k_B T\xi}{6\pi\eta L} \tag{4}$$

where D^{∞}_{self} is the diffusivity of water at the thermodynamic limit, ξ is a constant equal to 2.837297, η is the shear viscosity computed from Eq. (1), and L is the edge length of the simulation box.

The cohesive energy (intermolecular energy) among bitumen components was calculated to study cohesion of bitumen in the presence of water. It was defined as the sum of the intermolecular energy among only the bitumen components; interactions of water were omitted in this calculation. The *group/group* compute command in LAMMPS was used to distinguish between intramolecular and intermolecular contributions to van der Waals (i.e., LJ) energies that were computed directly between pairs. This entails an assumption that no molecule interacts directly with a periodic image of itself. Distinguishing between intramolecular and intermolecular contributions to Coulomb energy requires additional nuance. For atoms closer than a transition distance to each other, a direct pairwise computation of Coulomb energy can make this distinction. The long-range contribution to the Coulomb energy (PPPM) [46] accounts for interactions that arise over longer distances. By using reciprocal space to compute interactions between an atom and all other atoms beyond the transition distance, it indirectly includes interactions between a molecule and its infinite number of periodic images. Though these images arise from the same parent molecule, and thus would be categorized as intramolecular, their long-range Coulomb contribution corresponds to interactions between separate molecules within the framework of periodic boundary conditions.

To separate intramolecular and intermolecular contributions to the long-range Coulomb energy, the transition distance between a direct Coulomb energy calculation and a long-range (PPPM) calculation was increased to 25 Å in a separate simulation of an LG14 model with three times the number of atoms, which had an equilibrated box length larger than 50 Å. Because all bitumen molecules have a maximum intramolecular atom–atom separation that is less than 25 Å, the entire intramolecular electrostatic energy was calculated by partitioning the direct Coulombic energy. All of the long-range Coulomb energy contribution was thus assumed to be intermolecular. This includes the interactions between a molecule and its periodic images that arise over all length scales that are incorporated into the PPPM long-range Coulomb approach.

3. Results

3.1. Hydrogen bonding in water–bitumen systems

The presence of water hydrogen bonding was evaluated in order to assess how its extent affects diffusion mechanisms. Fig. 2(a) shows a representative MD simulation snapshot (using unwrapped coordinates) of a bitumen system with 0.93 wt% water content. The three distinct types of hydrogen bonds that occur in water–bitumen systems, i.e., bitumen–bitumen, water–bitumen, and water–water hydrogen bonds, are shown in Fig. 2(b), (c), and (d), respectively. A water molecule is capable of hydrogen bonding to a molecule of bitumen and simultaneously to another water molecule. Five types of heteroatom-based functional groups (denoted in Fig. 1) in the LG14 bitumen model [27] participate in bitumen–bitumen or water–bitumen hydrogen bonds. The simulation box contains 2 pyrrole (NA), 8 pyridine or quinoline (NC), 3 phenol (OHp), 5 ether (OS), and 37 thiophene (SA) of these heteroatom-based groups.

The numbers of hydrogen bonds of each type were counted in each saved configuration and were averaged over the sampling duration and subsequently over all five independent simulations. Fig. 3 shows these average numbers of all three types of hydrogen bonds for bitumen containing up to 1.76 wt% water over the temperature range 298–533 K. As can be seen in Fig. 3(a), there are 0.4–1.4 hydrogen bonds between bitumen components in a system without water for the considered temperatures. This range decreases to 0.2–0.8 bitumen–bitumen hydrogen bonds at 0.11 wt% water and decreases further to 0.1–0.6 hydrogen bonds at higher water contents. Few bitumen–bitumen hydrogen bonds occurred during most of the simulations. This indicates that hydrogen bond energy is not strong enough to favor the few bitumen–bitumen configurations that incorporate a hydrogen bond, compared to all other configurations with similar energies yet without the specificity of a hydrogen bonding geometry. The decrease in the number of bitumen–bitumen hydrogen bonds with the presence of water may be due to higher attractive forces between water and bitumen molecules, which causes bitumen–bitumen hydrogen bonds to be replaced by water–bitumen hydrogen bonds. The small size of water enables relative ease for it to achieve hydrogen bonding configurations near bitumen; this can also play a role.

An increasing presence of water leads to sharp increases in the numbers of water–bitumen and water–water hydrogen bonds, as shown in Fig. 3(b) and (c), respectively. With 2 water molecules in the box (0.11 wt%), at least one typically hydrogen bonded to a bitumen molecule at temperatures up to 393 K. At 443 K, the average number

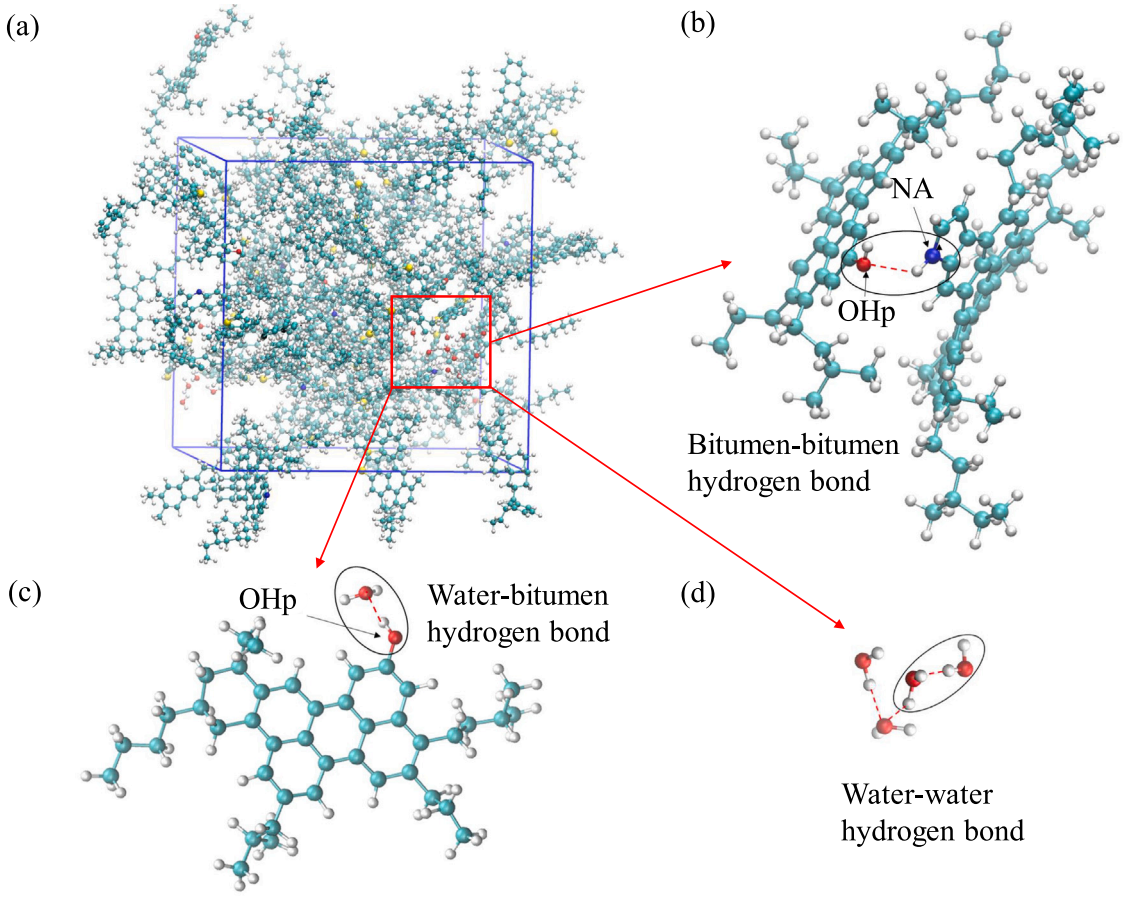

Fig. 2. Snapshots of (a) a water–bitumen system with 0.93 wt% water content, (b) a bitumen–bitumen hydrogen bond between asphaltene-phenol and asphaltene-pyrrole, (c) a water–bitumen hydrogen bond, and (d) three water–water hydrogen bonds at 313 K. A red dashed line represents a hydrogen bond between two molecules. NA and OHp are heteroatom-based functional groups in bitumen, as shown in Fig. 1. Color code for atoms: carbon (cyan), hydrogen (gray), nitrogen (blue), oxygen (red), and sulfur (yellow). (For interpretation of the references to color in this figure legend, the reader is referred to the web version of this article.)

of 0.55 corresponds to one hydrogen bond in just under every two configurations. A water–bitumen hydrogen bond occurred approximately once per 5 configurations at 533 K. With 16-fold increases in water content, the number of water–bitumen hydrogen bonds rose by factors of 4.5 times (at 298 K) to 11 times (at 533 K).

In contrast to bitumen–bitumen, the number of hydrogen bonds formed among water molecules is significantly affected by the temperature of the system. Fig. 3(d) shows the average number of hydrogen bonds per water molecule. This was calculated by summing the number of water–bitumen hydrogen bonds and twice the number of water–water hydrogen bonds, and then dividing by the total number of water molecules. At 533 K (the highest temperature), the number of hydrogen bonds per water molecule increases from ca. 0.1 to 0.7 as the water content increases from 0.11 to 1.76 wt%, while at 443 K and 393 K, this normalized number of hydrogen bonds becomes larger. Over temperatures of 298–353 K, the number of hydrogen bonds per water molecule increases from ca. 0.9 to 2.5. This clearly shows an increase in hydrogen bonding interactions among water molecules at lower temperature and with higher water content.

Water that forms hydrogen bonds with other water molecules, with bitumen components, or with both is commonly referred to as bound water. Water that does not participate in hydrogen bonding of any kind is referred to as free water (unbound individual water molecules). Fig. 4(a) shows the free water content as a function of the total water content in simulated bitumen at temperatures ranging from 298 K to 533 K.

At lower temperatures (298–313 K), increasing the total water content in bitumen has limited influence on free water. As shown in Fig. 4(a), the free water content decreases slightly with increased water content, though the decrease is within the range of the fluctuations. This suggests that the equilibrium free water content is obtained in the bitumen system with 0.11 wt% water, and thus an increase in total water content cannot increase the free water content further. At the system size employed here, this free water content corresponds to fewer than one water molecule per simulation box per snapshot.

At 353–443 K, free water content initially increases with increased water content in the system and reaches maxima of 0.041%, 0.092%, and 0.256%. These correspond to approximately 1, 2, and 5 free water molecules, respectively. After the maximum, a slight decrease is observed. At the highest temperature (533 K), free water increases monotonically with the water content in the system. A maximum free water content has not been reached by the highest simulated water content of 1.76 wt%.

As a simple model, we consider an energetic cost ΔE for a water molecule to be free rather than hydrogen bonded. At constant temperature, this suggests a probability density proportional to $\exp(-\Delta E/k_B T)$ for free water compared to bound water. Fig. 4(b) shows the maximum free water content at each temperature as an Arrhenius function. The logarithm of maximum free water content in bitumen varies approximately linearly with the inverse temperature. The slope suggests an energy cost of 9.4 kJ/mol for a water molecule to be free, i.e., to break from a hydrogen bonding network. Hydrogen bonding will be prevalent even at higher pavement temperatures of 64 °C, where thermal energy $RT \sim 2.8$ kJ/mol is much lower than this energy cost for a water molecule to be free.

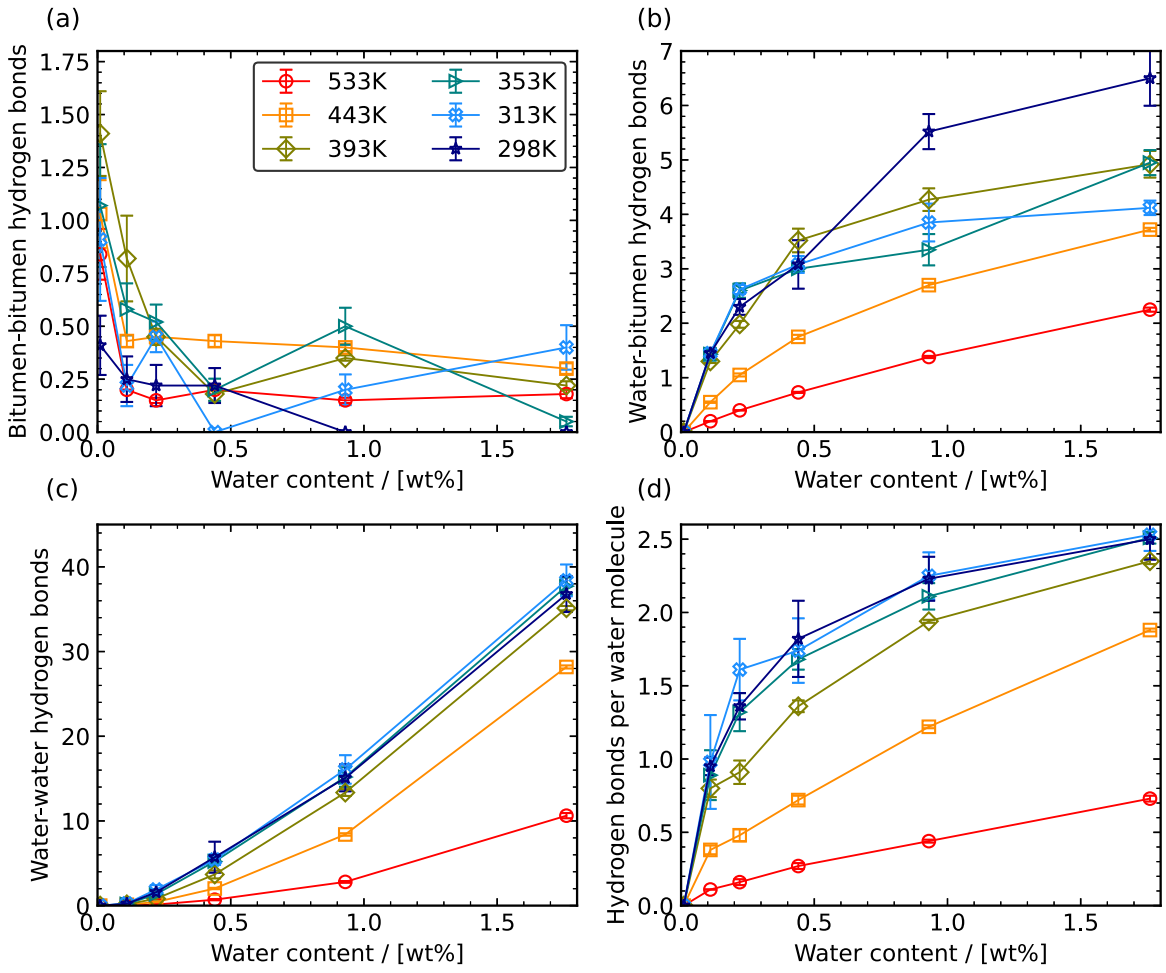

Fig. 3. Average number of (a) bitumen–bitumen hydrogen bonds, (b) water–bitumen hydrogen bonds, (c) water–water hydrogen bonds, and (d) hydrogen bonds per water molecule as a function of the water content.

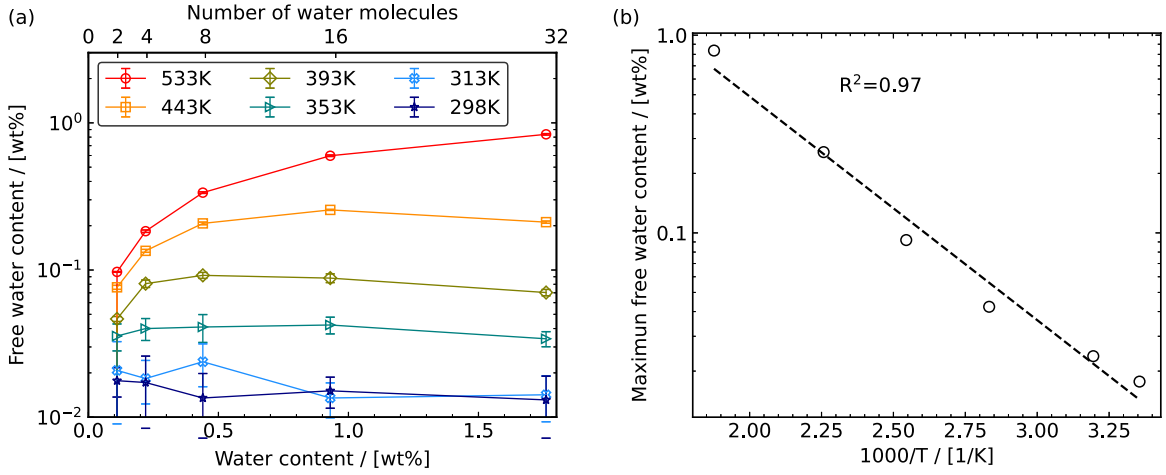

Fig. 4. (a) Free water content as a function of the water content in bitumen in the temperature range of 298–533 K, (b) maximum free water content as a function of temperature.

Functional groups in bitumen have different propensities to hydrogen bond with water. The LG bitumen model contains only 5 of the many possible functional groups, as depicted in Fig. 1. The fraction of hydrogen bonds between water and a specific functional group is computed as the ratio of the number of hydrogen bonds between water and this functional group to the total number of water–bitumen hydrogen bonds. Sometimes a single water molecule contributed hydrogen bonds to multiple bitumen functional groups. Each such hydrogen bond contributes separately to these fractions.

Fig. 5 distinguishes among the hydrogen bonds between water molecules and different functional groups. Water molecules form hydrogen bonds mainly with the NA, NC, and OHp functional groups. Among all functional groups, OHp and NA provide more of the water–bitumen hydrogen bonding sites, despite their lower concentrations

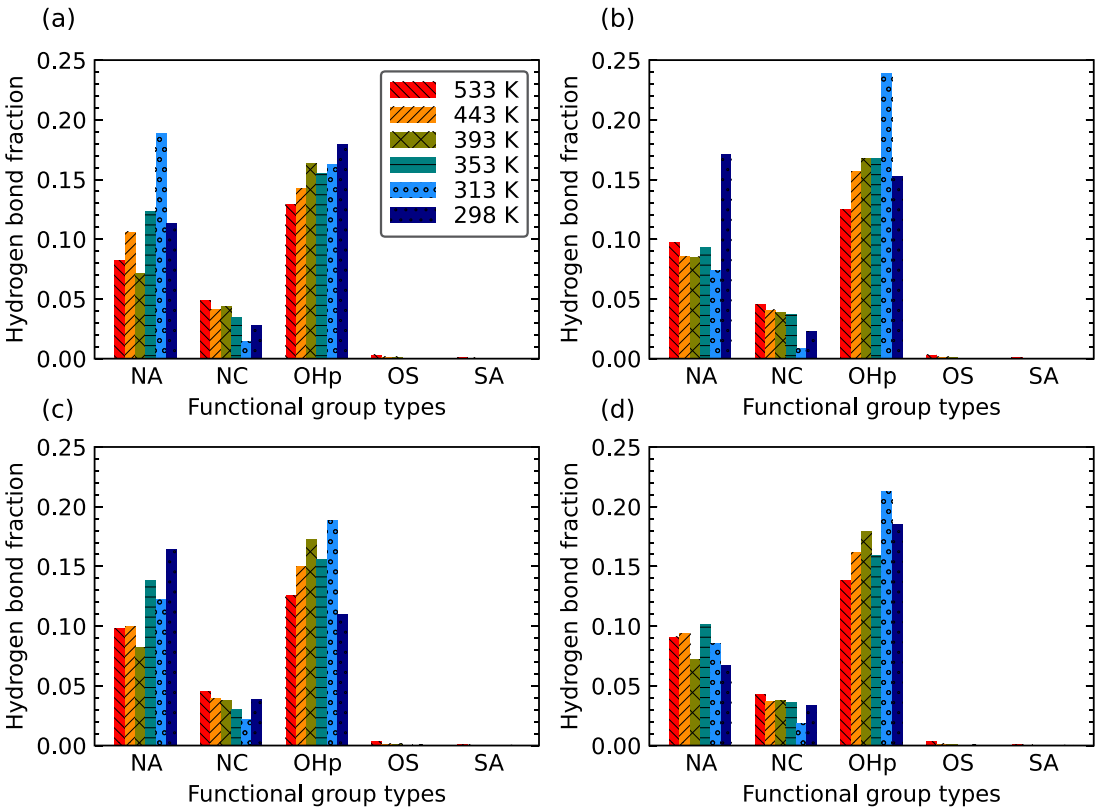

Fig. 5. Distributions of hydrogen bonds between water and various types of functional groups in bitumen at water contents of (a) 0.11 wt%, (b) 0.22 wt%, (c) 0.44 wt%, and (d) 0.93 wt%. NA, NC, OHp, OS, SA are heteroatom-based functional groups that are shown in Fig. 1.

compared to NC and SA. Fig. 5(a) – (d) show that, in most cases, the distribution of hydrogen bonds based on functional groups remains similar regardless of changes in water content.

3.2. Water clusters

Water clustering describes the aggregation of water molecules via hydrogen bonding. Fig. 6 shows the size distributions of water clusters for all water–bitumen systems as a function of temperature. The cluster fraction indicates the ratio of the number of water clusters of one size to the total number of water clusters. Free water is excluded from this calculation, so the smallest cluster size is two water molecules.

Three types of cluster size distributions are revealed in Fig. 6, namely monotonically decreasing, bimodal, and multi-modal distributions. At 533 K, the fraction of water clusters shows a monotonic and smooth decrease with increasing cluster size for all water–bitumen systems. At 443 K, the distributions in bitumen systems with water contents of 0.22–0.93 wt% also decrease monotonically, while a bimodal distribution is observed for the system containing 1.76 wt% water. After an initial decrease, this distribution has a local peak for a cluster size of about 28 molecules. Water clusters with sizes between 5 and 24 are rare. Similar phenomena are observed for the water–bitumen systems at 393 K and 353 K. The systems with low water content exhibit a monotonically decreasing number fraction of clusters of increasing size, and a bimodal distribution is observed with increasing water content. For the water–bitumen systems with a bimodal distribution, some of the water molecules form water clusters with small sizes up to ca. 5 water molecules, and the rest form large water clusters with sizes as large as the maximum number of water molecules in the systems. The absence of water clusters with intermediate sizes suggests that water molecules either form scattered clusters with small sizes or form one large cluster. Essentially, due to the overall hydrophobicity of bitumen, only a limited number of water molecules are able to dissolve in bitumen, and the additional water molecules tend to form a separate water phase. A particular water content exists that serves as a threshold above which phase separation occurs.

The water content at which the bimodal distribution first occurs is higher at higher temperatures. For the water–bitumen systems at 353 K, 393 K and 443 K, the presence of a bimodal distribution appears by water contents of 0.44 wt%, 0.93 wt%, and 1.76 wt%, respectively. This indicates a higher dissolution of water clusters with small sizes in bitumen at higher temperatures. It is consistent with the increase in free water content that is depicted in Fig. 4.

For water–bitumen systems at lower temperatures, i.e., 313 K and 298 K, a multimodal water cluster distribution is obtained in which water clusters form at various sizes that range from two to the maximum number of water molecules in bitumen. The presence of water clusters that contain nearly all water molecules in the systems indicates the same phase separation mechanism as previously described for higher temperatures. However, multiple peaks at low temperatures in Fig. 6 imply a more complex water clustering behavior. From another perspective, the larger error bars of cluster fractions at the lowest temperatures can potentially indicate an insufficient sampling time, which leads to different configurations and water cluster distributions among the five independent runs. In this regard, a bimodal water cluster distribution mode similar to the one at higher temperatures could potentially occur for water–bitumen systems at 313 K and 298 K when simulation sampling times even longer than 600 ns are applied.

3.3. Water radial distribution function

To investigate the positions of water molecules further, the RDFs for bitumen functional groups and water in the systems with 0.22 wt% and 0.93 wt% water were computed. The position $r = 0$ in Fig. 7 corresponds to atom OW, the oxygen atom of water, and $g(r)$ indicates the presence of heteroatoms in polar functional groups, as labeled

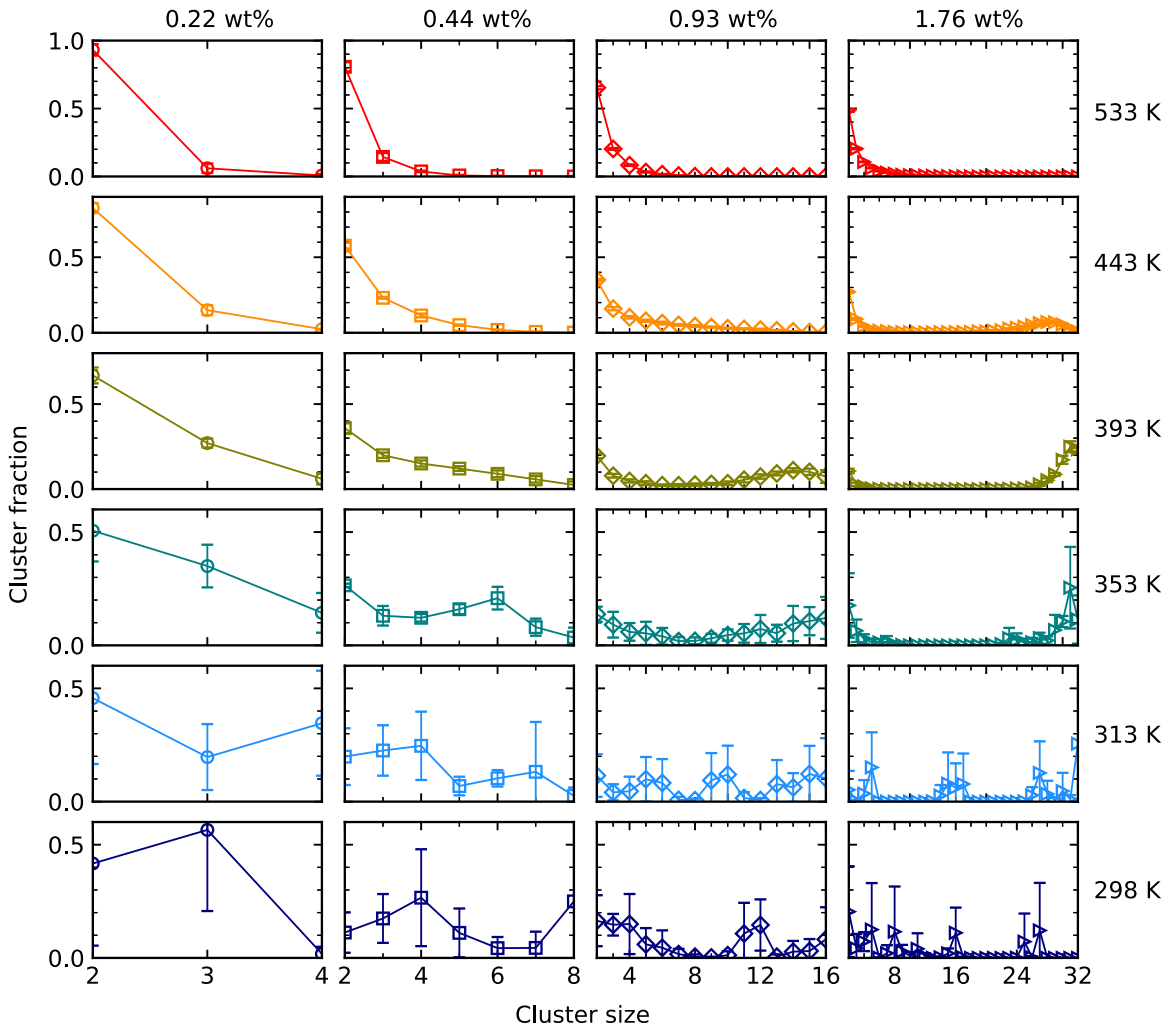

Fig. 6. Distributions of water cluster sizes for bitumen systems with various water contents (columns) at various temperatures (rows). The maximum cluster size shown equals the number of water molecules in the simulation box.

in Fig. 1, or of atom OW, the oxygen atom of water. Because RDF is a tabulation of pair distances and their relative probabilities, this separation can be interpreted equivalently as the distribution of water around heteroatom functional groups.

The location of the first sharp peak is at ca. 2.9 Å for all RDFs, which is consistent with hydrogen bonds between water molecules and these functional groups. The RDF regions of OW-OW exhibit high intensities over ranges from the first peak (2.9 Å) to about 6 Å for the system with 0.22 wt% water and to ca. 10 Å for the system with 0.93 wt% water. This suggests a very high density of water neighbors, namely water clustering. Similar regions of intensities with $g(r) \gg 1$ are found for the RDFs of OHp–OW and NA–OW up to the same concentration-dependent separations, while intensity is less high for NC–OW. At larger separations, the local densities of OW–OW separations are suppressed compared to the average density, i.e., $g(r) < 1$ (Fig. 7 insets). This provides further support for water clustering because it shows that water molecules are very close to each other or are farther away than the maximum length scale that is probed by the simulations (i.e., half a box length). Findings of $g(r) < 1$ at long separations for OW–OHp, and for OW–NA to some extent, support a description of these clusters as each being in the vicinity of bitumen heteroatoms. The larger RDF peaks for OHp and NA, compared to NC and especially to OS and SA, are consistent with the distributions of hydrogen bonds between water and various types of functional groups depicted in Fig. 5.

3.4. Water diffusion in bitumen

Interpretations of gravimetric and spectroscopic experimental measurements of water transport in bitumen suggest differences in diffusion rates for water that remains free compared to water that forms hydrogen bonds and water clusters [17,19,21]. To analyze this effect in the MD results, mean-squared displacements (MSDs) of water molecules for all water–bitumen systems were computed for correlation times (also known as time differences) of 0.1 ps to over 100 ns. Results presented in Fig. 8 indicate three regimes. The first represents the ballistic regime in which molecules move freely without having a collision, and MSD $\sim t^2$. The second regime shows anomalous diffusion in which MSD $\sim t^n$ with slope $n < 1$ on a log–log plot. The third regime describes the diffusive mode in which molecules escape this trapped domain and perform a random walk with MSD $\sim t$. These regimes exhibit different trends with increasing water content as denoted by arrows in the figure.

Fig. 8 shows that water molecules in bitumen systems with lower water content move through the first regime more rapidly. MSDs are higher at the initial time separation, and the diffusion exponent has already begun to decrease from its short-time $n = 2$ asymptote (inset, dashed line), particularly for lower water content. Lemarchand et al. [28] found the same trends in their simulations of water in Cooee model bitumen. As shown in Fig. 3(d), the number of hydrogen bonds per water molecule increases with higher water content, which indicates an increase in hydrogen bonding interactions among water

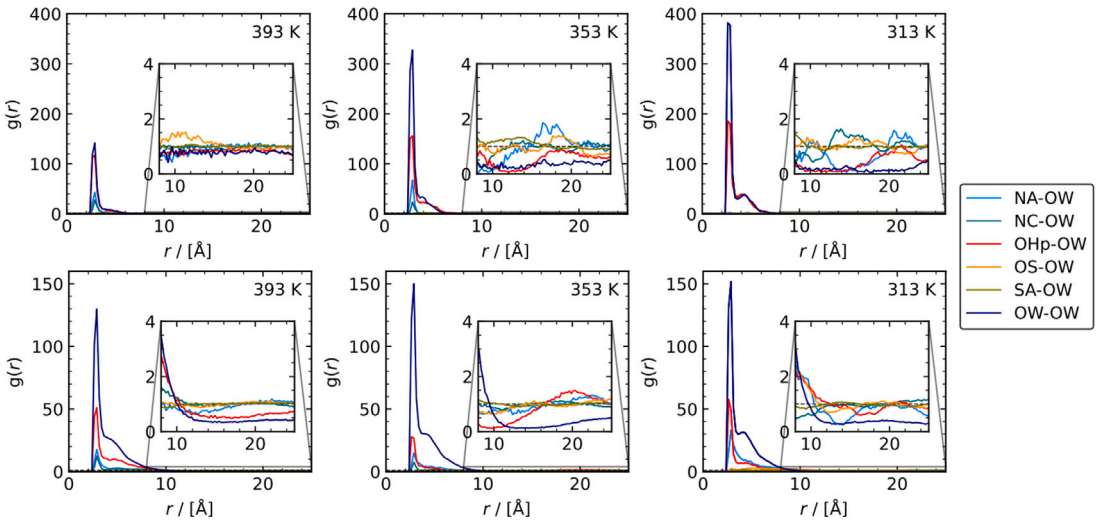

Fig. 7. Radial distribution functions of water–water and water–bitumen functional groups for systems with water contents of 0.22 wt% (upper row) and 0.93 wt% (lower row) at different temperatures (columns). OW represents the oxygen atom of water and NA, NC, OHp, OS, SA are heteroatom-based functional groups as shown in Fig. 1.

molecules. This increased interaction leads to a slower ballistic motion of water molecules.

An anomalous second regime is found over time spans of ca. 10^{-3} to at least 10^{-1} ns in the water–bitumen systems, with the endpoint occurring at longer times for lower temperatures. Anomalous diffusion indicates motion within kinetically constrained regions [68], which means a molecule is blocked from diffusing further until a rare event opens a new path. A higher water MSD in the anomalous regime is observed for the systems with higher water content. This trend can be explained by micro-phase separation between water and bitumen. Water molecules that are surrounded by bitumen molecules move within a small region before being blocked. Water molecules within a water cluster are able to diffuse through the entire cluster before being blocked by the surrounding bitumen.

Higher water content leads to larger water cluster size as already discussed in section 3.2. For water molecules in larger clusters, a longer time is required to escape a cluster and to show diffusive motion. A later initiation of the third regime (MSD $\sim t$) is thus observed for systems with higher water content. As a result, the larger cluster size leads to a lower diffusion coefficient of water. It is important to note that this initiation time increases significantly at lower temperatures, such as from 1 to 10 to over 100 ns at 313 K for 0.11, 0.44, and 0.93 wt%, respectively. Simulations [38,69] that span only shorter times than this crossover can therefore only capture the ballistic and anomalous dynamics. True diffusion is not yet in effect even if a plot with linear axes of MSD vs. correlation time can be fit with a straight line over a limited time domain.

The logarithmic axes of Fig. 8 facilitate illustrating how imposing a linear fit, $\log \mathrm{MSD} = \log 6D + \log t$, at too short of a correlation time will suggest a shift of the $n = 1$ line (dashed) to earlier times. This "left shift" of the fit leads to a higher MSD at $t = 1$, which implies an artificially high diffusion coefficient. Long enough simulations are required in order to have confidence in a reported diffusion coefficient. Prior simulations of water that reached the diffusive regime in bitumen [28] also showed a decrease in the diffusion coefficient of water as water content increased.

To illustrate the effects of hydrogen bonding and water clustering on water diffusion dynamics, examples of distinct MSD patterns in a simulation at 313 K are shown in Fig. 9. The MSDs of all water molecules (16 water molecules labeled as 1–16 in a bitumen system with 0.93 wt% water content) are plotted individually. MSDs between distinct time points $\Delta t = (t_j - t_i) > 0$ evolve in four patterns.

Many water molecules remain in the same cluster through most of the simulation. Water molecules 3, 5, 6, 9, 12, 13, 14, and 15 experience similar MSDs and show similar diffusion dynamics. The upper snapshot inset in Fig. 9 visualizes that these water molecules belong to the same water cluster (group 1). Another MSD pattern is shared by water molecules 1, 2, 7, and 16 (group 2). To verify that water molecules with similar MSDs are in the same water cluster throughout the simulation, the probabilities of water molecules being in the same water cluster group were calculated. These are defined as the ratio of the number of snapshots in which water molecules belong to the same cluster group to the total number of snapshots. Molecules 3, 5, 6, 9, 12, 13, 14, and 15 are in group 1 for 97.6% of all snapshots. This probability is 92.5% for water molecules 1, 2, 7, and 16 in group 2. The probabilities that water molecules in Fig. 9 are free or have certain types of hydrogen bonds (water–bitumen, water–water, or both) were also calculated as time averages and are presented in Table 1. The probabilities of being free, experiencing water–bitumen, and experiencing water–water hydrogen bonding are similar for water molecules in the same cluster group.

Another pattern involves diffusing water molecules belonging to a distinct water cluster less frequently. Molecule 10 was found to be part of group 1 in 95.4% of the simulation snapshots, lower by 2.2% than other molecules in the same cluster. A representative series of consecutive simulation snapshots corresponding to ca. 600 ps are shown in Fig. S10. During this short simulation period, molecule 10 moves away from group 1 and later rejoins this same group. Visualization of the full trajectory shows that this pattern recurs. The similar MSDs of molecule 10 and group 1 for $\Delta t < 1$ ns correspond to their shared dynamics as a group. The greater MSD of molecule 10 at longer correlation times compared to the MSD of molecules in group 1 is a result of its higher mobility when it is outside of the cluster.

Some water molecules depart from a water cluster and diffuse elsewhere. The faster diffusion of molecule 4, compared to group 2, can also be explained by its higher probability of being free and its lower probability of remaining in group 2 (87.7%). Visualization of the full trajectory indicates that molecule 4 diffuses far away from group 2 in some snapshots. Later, it encounters and joins a periodic image of the same group. The probabilities for molecule 11 to form water–bitumen and water–water hydrogen bonds are between the probabilities that are found for molecules in group 1 and group 2. Molecule 11 is in group 1 and group 2 for 37.0% and 56.6% snapshots, respectively. Its higher MSD compared to group 1 and group 2 is a consequence of its higher mobility.

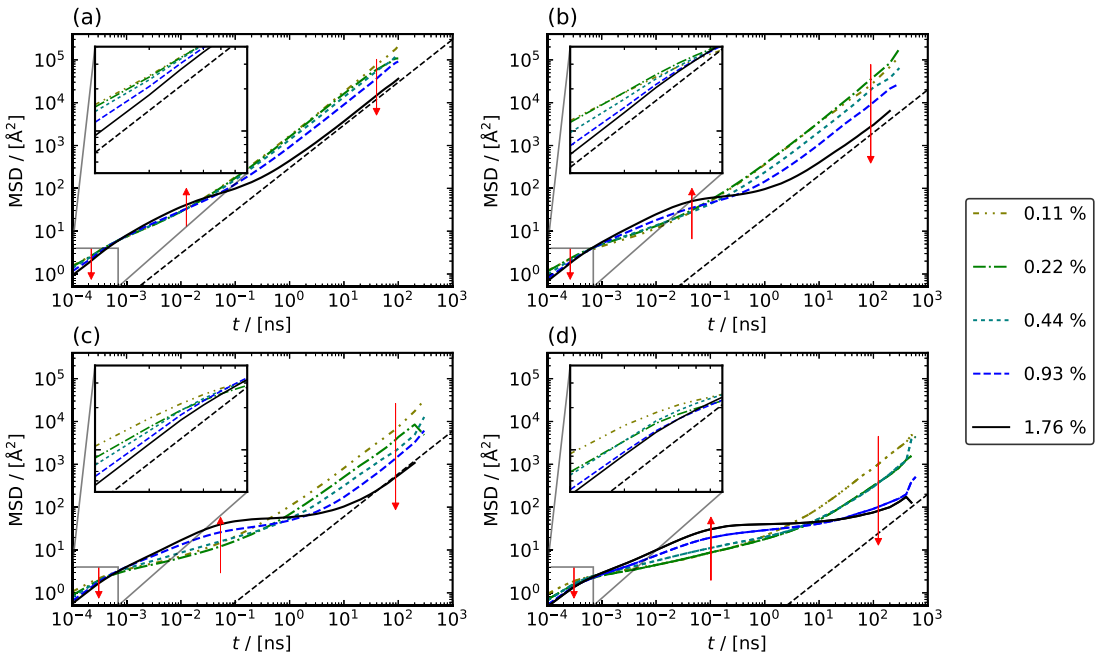

Fig. 8. Mean-squared displacements of water molecules for bitumen systems with water contents from 0.11 wt% to 1.76 wt% at temperatures of (a) 443 K, (b) 393 K, (c) 353 K and (d) 313 K. Black dashed lines in each panel (inset) have a slope of one (two). Arrows indicate trends of MSDs with increasing water content at different time scales.

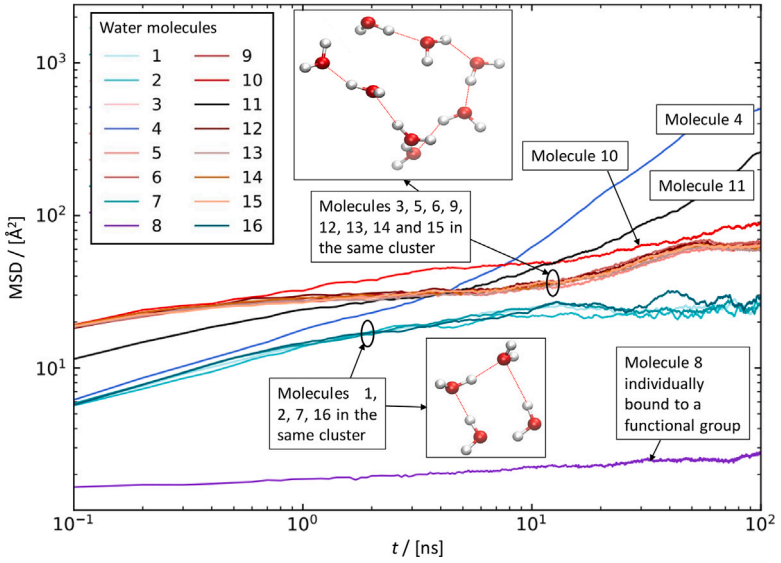

Fig. 9. MSDs as a function of correlation time for all individual water molecules in a bitumen system with 16 water molecules (0.93 wt% water content) at 313 K. Insets depict water clusters within a representative simulation snapshot at the elapsed time indicated (gray atoms denote hydrogen, red atoms denote oxygen). (For interpretation of the references to color in this figure legend, the reader is referred to the web version of this article.)

The final pattern is the slow diffusion experienced by molecule 8. In 97% of snapshots, this molecule is hydrogen bonded to functional groups of bitumen. Due to the slower diffusion of bitumen components compared to water, this water molecule diffuses more slowly.

In terms of the three diffusion regimes, Fig. 9 shows that water molecules that are in water clusters and or that are hydrogen bonded to bitumen exhibit only anomalous diffusion over the correlation times shown. Only the water molecules that manage to escape water clusters and diffuse elsewhere (molecules 4 and 11 in this example) exhibit true diffusive motions. Even molecule 10 exhibits a root-mean-squared displacement smaller than 10 Å over $\Delta t \sim 200$ ns at 313 K.

The self-diffusion coefficients of water in the bitumen systems with various water contents and at different temperatures are shown in Fig. 10. They are fit to the Arrhenius equation

$$\ln D^{\infty}_{\text{self}} = \ln D_0 - \frac{E_A}{RT} \tag{5}$$

where D^{∞}_{self} is calculated from MSD and corrected for finite-size effects according to Eqs. (3) and (4), D_0 is a constant, E_A is the activation energy of self diffusion, R denotes the universal gas constant, and T is the temperature. The fitted parameters are shown in Table 2. In Fig. 10, it can be seen that increasing water content reduces the self-diffusion coefficient of water. As discussed earlier, lower temperature and higher water content in the system cause increases in the numbers of hydrogen bonds and of water clusters, which result in a slower diffusion rate and a higher activation energy. In all cases, the activation energy for

Table 1
Probabilities for water molecules to stay as free or to form water–bitumen (bit-wat) or water–water (wat-wat) hydrogen bonds in the water–bitumen system with 16 water molecules (0.93 wt% water content) at 313 K. Water molecules hydrogen bonded to both water and bitumen were defined as the bit-wat-wat group.

	Group-1									Group-2						
Water molecule	3	5	6	9	12	13	14	15	10	1	2	7	16	4	11	8
Free	0.01	0.01	0.01	0.01	0.01	0.01	0.01	0.01	0.03	0.01	0.00	0.01	0.01	0.03	0.01	0.03
Bit-wat	0.00	0.00	0.00	0.00	0.00	0.00	0.00	0.00	0.00	0.04	0.04	0.05	0.05	0.06	0.03	0.97
Bit-wat-wat	0.12	0.12	0.15	0.12	0.12	0.11	0.13	0.13	0.12	0.47	0.40	0.48	0.51	0.44	0.34	0.00
Wat-wat	0.87	0.87	0.84	0.87	0.87	0.87	0.86	0.85	0.84	0.48	0.56	0.46	0.43	0.47	0.62	0.00

Table 2
Concentration-dependent self-diffusion coefficient and corresponding Arrhenius parameters for water in bitumen.

Water content/[wt%]	0.11	0.22	0.44	0.93	1.76
D^{∞}_{self} at 313 K/[m^2/s]	1.43×10^{-11}	6.05×10^{-12}	2.01×10^{-12}	8.02×10^{-13}	4.01×10^{-13}
D_0/[m^2/s]	1.58×10^{-4}	6.29×10^{-4}	2.96×10^{-3}	9.15×10^{-3}	1.15×10^{-2}
E_A/[kJ/mol]	41.4	47.0	53.5	58.9	62.2

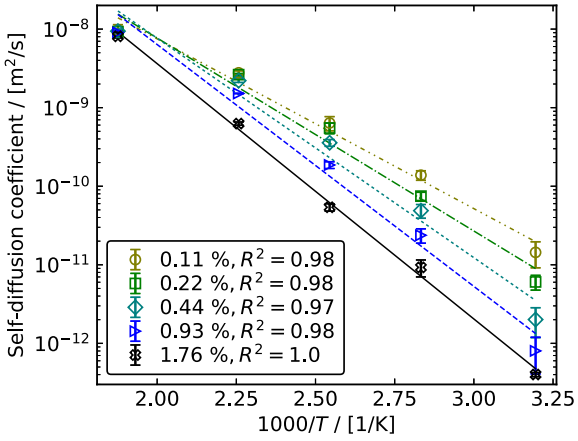

Fig. 10. Self-diffusion coefficients of water in water–bitumen systems with various water contents as a function of temperature. Lines indicate Arrhenius fits.

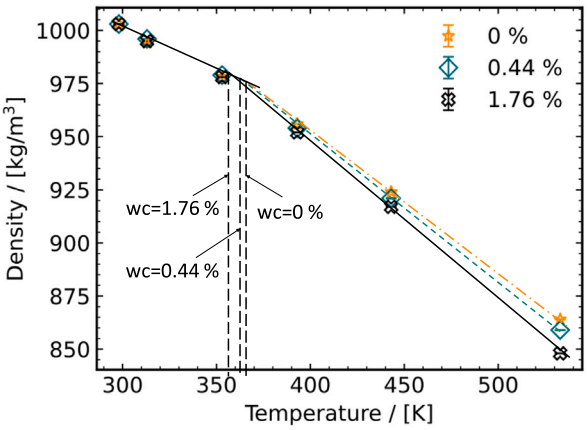

Fig. 11. Densities of simulated water–bitumen systems with various water contents as a function of temperature. Sloped lines are linear fits of density vs temperature. Vertical dashed lines indicate the intersections of density linefits.

diffusion is significantly greater than the energetic cost for a water molecule to become free of a water cluster.

3.5. Bitumen properties in the presence of water

So far, we have shown that water molecules in bitumen can be free, hydrogen bonded to bitumen, or hydrogen bonded to other water molecules, and the diffusion coefficient varies significantly for these water states. In this section, density, viscosity, and cohesive energy of water–bitumen systems are computed to evaluate the effects of hydrogen bonding and water clustering on bitumen properties.

The densities of the water–bitumen systems are shown in Fig. 11. The bitumen density computed at 298 K without water is 1004 kg/m^3, which is close to the density of 1000 kg/m^3 reported by Li and Greenfield [27] from shorter simulations (same bitumen model as in this work) and 997 kg/m^3 reported by Khabaz and Khare [70] for the same model composition simulated with the general AMBER force field [71]. The interpolated simulated density is 3.5% smaller than the experimental value of 1030 g/cm^3 at 333 K [72]. The thermal expansion coefficient $\alpha = -\frac{1}{\rho}\left(\frac{\partial\rho}{\partial T}\right)_P = 5.5\times10^{-4}$ K^{-1} from simulation is slightly smaller than the 5.9×10^{-4} reported from experiments [72].

The density of the simulated water–bitumen systems depends on water content and temperature. The density of water at 1 atm is 972–997 kg/m^3 at temperatures from 353 K to 298 K, which is similar to that of bitumen. Therefore, no significant changes are expected for bitumen density upon ideal mixing with water at lower temperatures. At temperatures higher than 353 K, the addition of water decreases the water–bitumen density.

A glass transition is indicated by a change in slope of density as a function of temperature. The transition temperature (T_g) is determined by the intersection of linear fits that represent glassy and rubbery regimes. The computed T_g of ca. 360 K is significantly higher than the experimental value of ca. 250 K [73]. A T_g of 350 K was identified in previous MD simulations [70] of the LG14 bitumen model that computed densities at temperatures from 600 to 80 K with a step of 20 K. One possible reason for the divergence of computed T_g from experimental values is the much higher cooling rate of MD simulations compared to experimental tests [70]. For polymeric materials, a higher experimental cooling rate results in a higher glass transition temperature (T_g) and a lower density because of insufficient time for structural relaxation [74]. Consequently, the higher cooling rate used in molecular simulations yields a higher T_g than what is typically observed in experimental settings. Furthermore, a decrease in T_g with higher water content demonstrates a plasticization effect of water [75], which influences the relaxation and viscosity of bitumen systems, as discussed in the following section.

The viscosities of bitumen and water–bitumen systems are shown in Fig. 12. A decrease in viscosity with increasing water content is observed, which is consistent with plasticization, i.e., increasing water content can facilitate bitumen mobility, thus resulting in a lower viscosity. This can also be seen in the MSDs of the components of the integrated traceless pressure tensor in Figs. S11–S14 of the Supplementary Material. Higher water content leads to smaller MSD of stress.

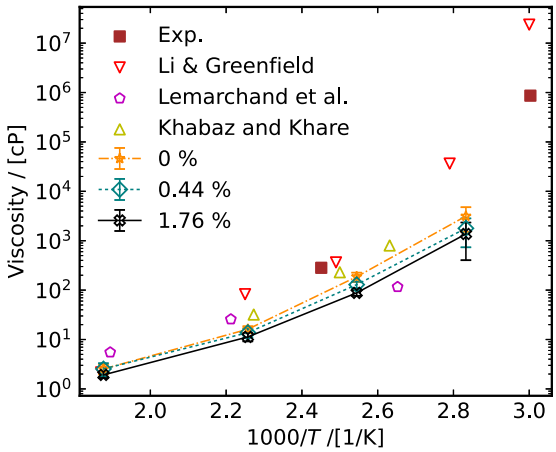

Fig. 12. Viscosities of water–bitumen and bitumen systems computed in this work and from the MD simulations reported by Li and Greenfield (AAA-1) [55], Lemarchand et al. (Cooee) [76], Khabaz and Khare (AAM-1) [41], and from experiments on SHRP AAA-1 bitumen [34].

Also, the long correlation times that are required until the eventual attainment of a log-scale slope of 1 indicate the long stress relaxation time scales that are required for the viscosity calculation to converge. The relaxation time scale already exceeds hundreds of nanoseconds at 393 K and is even longer at lower temperatures.

Fig. 12 also shows viscosities obtained from experiments [34] and from MD simulations reported by Li and Greenfield [55], Lemarchand et al. [76], as well as Khabaz and Khare [41]. Li and Greenfield [55] calculated viscosity directly at 533 K for the same bitumen model as used in the present work; those at other temperatures were scaled based on the rotational relaxation times computed from MD simulations. Lemarchand et al. [76] used the Cooee bitumen model and non-equilibrium MD (NEMD) simulations to compute shear viscosity. The viscosities reported by Khabaz and Khare [41] were computed using the NEMD method, the SHRP AAM-1 version of the LG14 bitumen model [27], and the general AMBER force field [71]. The computed viscosity at 533 K in this work agrees well with the value provided by Li and Greenfield [55]. Other viscosities directly obtained from the present MD simulations are lower than the inferred viscosities in Ref. [55]. Compared to the results of the present work, viscosities by Lemarchand et al. [76] are slightly higher at higher temperatures and are lower at lower temperatures. The viscosities computed in the present work are slightly lower than those computed by Khabaz and Khare [41] for simulated SHRP AAM-1. All the viscosities shown in Fig. 12 that are computed directly by molecular simulation are lower than typical experimental results. This could be due to limitations of the LG14 model in simulating bitumen. This 12-component bitumen model cannot incorporate the full range of molecule polarities and sizes that are present in real bitumen. The benzobisbenzothiophene that supplies much of the sulfur has a low molecular weight compared to most molecules in real bitumen, for example.

Fig. 13 shows the variation of bitumen cohesive energy as a function of water content at different temperatures. Adding water molecules in bitumen slightly decreases the cohesive energy of bitumen (negative cohesive energy is more favorable). This may be explained by water molecules replacing the initial bitumen–bitumen hydrogen bonds by forming water–bitumen hydrogen bonds (Fig. 3). Furthermore, nearest-neighbor bitumen–bitumen nonbonded interactions other than hydrogen bonding can be replaced by water–bitumen interactions, especially for the locations where water clusters occur (Fig. 7). This further weakens the interactions between bitumen components. The variation of cohesive energy with respect to water content does not show a clear dependence on temperature. Differences among the five independent simulations were smaller at higher temperatures; there, the relaxations are faster and the results are better converged.

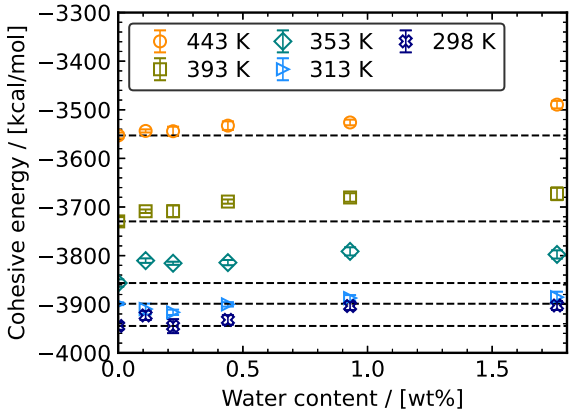

Fig. 13. Cohesive energy of bitumen components as a function of water contents at various temperatures.

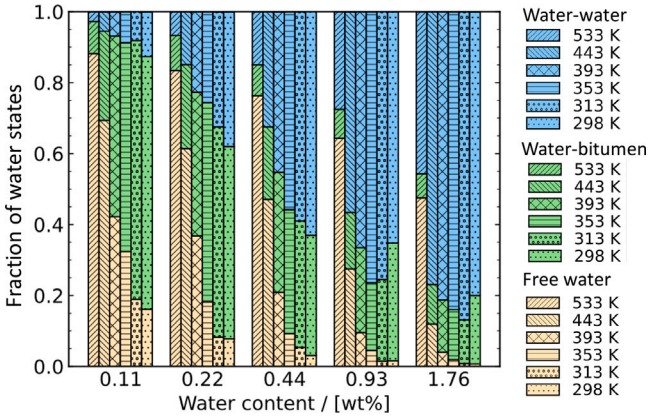

Fig. 14. Distribution of water hydrogen bonding states in bitumen: free water, water with water–bitumen hydrogen bonds, and water with water–water hydrogen bonds. Within each water content, temperature decreases from left to right.

4. Discussion: insight into water transport mechanisms at the macroscale from molecular simulation

Macro-scale water diffusion models invoke assumptions that absorbed water is present in both free and bound modes [17–19,21,22]. Results in the prior sections describe the dynamics of hydrogen bonding and diffusion of water. Our intent in this section is to interpret these simulation results and to provide insights in terms of how they impact the molecular interpretations that underlie these phenomenological approaches to moisture absorption, transport, and damage.

Three water hydrogen bonding states are revealed from the MD simulations by quantifying the types of hydrogen bonds: free water, water hydrogen bonded to bitumen, and water hydrogen bonded to water. The extent that water molecules experience each hydrogen bonding state and the ways that their diffusion dynamics can be interpreted via free and bound modes depend on both temperature and water content.

To characterize the water hydrogen bonding environment in bitumen further, the relative fractions of each state were calculated at all temperatures. Water molecules hydrogen bonded both to water and to bitumen are included in the category of water–bitumen hydrogen bonds. Results are depicted in Fig. 14.

The structures formed by absorbed water molecules relate qualitatively to the temperature-dependent extent that bitumen molecules can fluctuate in orientation and shape. These affect the accessibility of hydrogen bonding sites. Figs. 3, 4, and 14 show that the distribution of hydrogen bonding configurations in bitumen is affected by both

temperature and water content. For bitumen systems at lower temperatures, only small absolute differences in the numbers of hydrogen bond types (Fig. 3) and in the free water content (Fig. 4) are observed with increasing water content. In water–bitumen systems at higher temperatures, a rise with temperature in the amount of free water is more apparent (Fig. 4). Simultaneously, a significant decrease is observed in all types of hydrogen bonds with increasing temperature. Combining these trends, there are fewer hydrogen bonds and more free water molecules with increasing temperature. In the lower temperature regime, changes in temperature have smaller effects on hydrogen bonds and free water contents. Together, these results indicate a higher solubility of water in bitumen and a lower probability to form large water clusters at higher temperatures (Fig. 6).

The overall number of hydrogen bonds increases with water content (Fig. 3), which results in more water clusters with larger cluster sizes, as shown in Fig. 6. The cluster size distribution reveals that large water droplets form in the simulated bitumen at water concentrations higher than 0.93 wt%, 0.44 wt%, and 0.22 wt% at temperatures of 443 K, 393 K, and 353 K, respectively. Participating in hydrogen bonds is more energetically favorable for water (Fig. 4(b)), so very little water is required before a droplet forms. Similar results were reported by Lemarchand et al. [28], who found droplets for 5 water molecules in a simulation box of bitumen, the smallest concentration that they simulated.

Results from the distributions of hydrogen bonds between water and various types of functional groups (Fig. 5) and the RDFs (Fig. 7) provide additional information about where hydrogen bonds and water droplets were located within the simulated bitumen. These results show that the positions of hydrogen bonds and water clusters depend on the functional groups in bitumen. Among all types of functional groups in the simulated LG14 model, water clusters are mostly next to a pyrrole (NA) or phenol (OHp) group, as indicated by $g(r) < 1$ at large separations for these atom pairs, while some water clusters are near a pyridine (NC) group. From the perspective of the heteroatom, water molecules tend to be nearby rather than randomly distributed. Consequently, the type and fraction of heteroatom-based functional groups in bitumen are crucial factors that affect water clusters. These functional groups act like nuclei for the growth of clusters at high water contents.

In experiments, saturated moisture content varies with bitumen types [17,19,21], which vary in heteroatom content and thus in heteroatom bonding chemistry as consequences of the bitumen crude oil source and the production method employed. Cheng et al. [19] reported a positive relationship between water absorption and asphaltene fraction, which contains more heteroatom components than other SARA fractions. Within LG14 model bitumen, the polar sites that attract water are in distinct fractions. NA and OHp are exclusively in the asphaltene fraction and NC is exclusively in the resin fraction. Sulfide sulfur that can oxidize to sulfoxide is absent in the model. This discrete distinction between asphaltene and resin is a consequence of the relatively small number of distinct molecule types in the LG14 system rather than an accurate depiction of bitumen chemistry in general. Presence of NA and OHp among asphaltenes is consistent with an increased asphaltene fraction providing an increased opportunity for probable water–bitumen hydrogen bonding and water clustering sites. An increased number of these sites may lead to a higher water absorption in bitumens that differ in their distribution of SARA fractions.

At macroscopic scales, it can be expected that the majority of water would form large water droplets that accumulate around polar sites in bitumen. In this case, the macro-scale cohesion of bitumen could be seriously weakened. Furthermore, the polarity of aggregates is generally higher than that of bitumen [77]. Providing a higher concentration of polar sites on the aggregate surface makes water molecules more likely to form clusters at the bitumen-aggregate interface, which can lead to the degradation of adhesion between bitumen and aggregates. By forming water droplets inside bitumen and at the bitumen-aggregate interface, water transport can result in cohesive and adhesive failure.

In addition to polar functional groups (content of ca. 0.5–5 wt%), inorganic salts and metals (content in the range of 1–1000 ppm) [2] may also act as water clustering sites [17,78]. Salts and metals were not incorporated here. This is due in part to their low concentration; a single NaCl molecule added to the LG14 bitumen model would have a mass concentration of 1800 ppm. These trace elements in bitumen, along with functional groups at a bitumen-aggregate interface, may also act as nuclei for the formation of water clusters, potentially contributing to degradation within bitumen and at the bitumen-aggregate interface. Molecular simulations and experiments that focus on the water behavior of bitumen with varying concentrations of trace elements could provide insight into the effects of these trace elements on bitumen performance and durability.

The different diffusion dynamics of the water states offer insights into the assumptions in the diffusion models used for interpreting experimental data as well as into the physical meanings of different diffusion coefficients [17–19,21]. The diffusion rate of water is influenced by the extent to which it engages in hydrogen bonding and forms water clusters with other water molecules. Free water has the fastest diffusion rate, while water in clusters exhibits much slower diffusion dynamics. Water molecules hydrogen bonded to bitumen may be considered as completely immobile because their large-scale motions are confined to the diffusion of functional groups of bitumen.

MD simulation results for the self-diffusion coefficient of water in systems with low water mass fractions can be compared to the diffusion rate of the free water mode in diffusion models that are fit to data from experiments conducted close to the infinite dilution limit [17–19,21]. The self-diffusion coefficients of water in the systems with 0.11 wt% and 0.22 wt% water contents at 313 K are 1.43×10^{-11} m^2/s and 6.05×10^{-12} m^2/s, respectively. The computed self-diffusion coefficients are close to the experimental values of 3.2×10^{-12} m^2/s–4.6×10^{-12} m^2/s for free water that were previously measured by Ma et al. [18], in which the water concentration is ca. 0.15 wt%. Other experimental studies [17,19] have reported a much lower diffusion coefficient of the free mode i.e., in the range of 10^{-15} – 10^{-13} m^2/s. In Ref. [19], the free water fraction is reported as ca. 0.4–0.9 wt% (the total water absorption is ca. 1.2–6.5 wt%), which is much higher than the free water fraction in the simulations, as shown in Fig. 14. The free and bound phases revealed in Ref. [19] may be considered as water molecules belonging to water clusters and hydrogen-bonded to polar sites of bitumen, respectively. Therefore, the lower diffusion coefficients obtained from these experiments could represent the diffusion rate of water clusters instead of free water molecules, as assumed in the diffusion models. Simulation results are consistent with slower diffusion at this higher water content, such as 4.01×10^{-13} m^2/s at 313 K for 1.76 wt%. Furthermore, the much lower free water fraction indicated in Fig. 14 makes gravimetric or spectroscopic measurements more sensitive to droplet dynamics than to the diffusion of isolated water molecules within bitumen.

Structure and diffusion results from MD simulations suggest that the bound mode in diffusion models [17–19,21] corresponds to water molecules that are hydrogen bonded to polar sites of bitumen or are clustered together via water–water hydrogen bonding. At temperatures commonly used in experiments (298 K and 313 K), and for lower water contents, the water molecules that form water–bitumen hydrogen bonds dominate the bound phase, which can be assumed as completely immobile. As the water content increases, additional water molecules mainly form water–water hydrogen bonds. At this water concentration, the "bound phase" should be considered as diffusing with a much lower diffusion coefficient. This interpretation can be related to macroscale studies of water diffusion in bitumen. In previous work, which investigated the thermodynamics and kinetics of moisture transport in bitumen using dynamic vapor sorption (DVS) [18], moisture diffusion was measured during exposure to air at 80% relative humidity (RH).

The Cluster model, which assumes that free water diffuses at a constant rate while clustered water remains immobile, showed the best performance in modeling the results. According to the Cluster model, the pseudo-diffusion coefficient (combining both free and clustered water) decreases with increasing water concentration. Findings from that experimental study corroborate well with the simulation results presented here, namely, higher water content leads to more water clusters with larger sizes, which leads to lower diffusion coefficients.

The physical properties of water–bitumen systems show that the presence of water in bitumen decreases its viscosity. As noted in sections 3.1 and 3.2, the soluble water concentration in bitumen (i.e., free water molecules and water molecules with small cluster sizes) is low, especially at lower temperatures. For the water–bitumen systems with high water contents, there are large water clusters (water droplets), which indicate a separated water phase. These clusters can increase the flexibility of bitumen and decrease its viscosity. The presence of water clusters also suppresses interactions between bitumen components and therefore weakens bitumen cohesion.

In summary, the results obtained here for the distributions of free water and water clusters via hydrogen bonding in bitumen, as well as their diffusion dynamics, provide in-depth insights into the diffusion mechanisms and assumptions involved in diffusion models that are used to infer diffusion coefficients from experimental gravimetric and spectroscopic data. At low water concentrations (such as 0.11 wt%), water molecules either freely diffuse in bitumen with a diffusion coefficient of ca. 10^{-12} m^2/s or are hydrogen bonded to polar sites, which can be assumed as immobile. As water concentration increases, water clusters occur and their sizes and fractions gradually increase until they become the dominant water phase (water concentration greater than ca. 0.5 wt%). The diffusion coefficients of these clusters depend on the cluster size and are in the range of 10^{-15}–10^{-13} m^2/s, or even lower. At this stage, the fraction of free water is small, and the remaining water outside clusters is hydrogen bonded to bitumen and is immobile.

5. Conclusions

To gain a molecular-level insight into the assumptions of water diffusion models for experimental analysis, and to provide an atomistic explanation of water-induced damage mechanisms in bituminous materials, water–bitumen systems with water contents ranging from 0 wt% to 1.76 wt% at various temperatures were investigated using MD simulations with durations up to 600 ns.

Three types of hydrogen bonds are found in the water–bitumen systems, i.e., bitumen–bitumen, water–bitumen, and water–water hydrogen bonds. Based on hydrogen bond types, three water molecular states are revealed: free water, water with water–bitumen hydrogen bonds, and water with water–water hydrogen bonds (water clusters). Some water molecules form hydrogen bonds with both bitumen and other water molecules. At lower water contents (compared to a solubility limit that increases with increasing temperature), water molecules are scattered inside the bitumen structure as free molecules or are hydrogen-bonded to bitumen. At higher water contents, most of the water molecules cluster together into large droplets via water–water hydrogen bonding, resulting in a phase separation between water and bitumen. The large water clusters tend to form at positions close to the pyrrole and phenol functional groups in bitumen. The type and content of functional groups are highly related to the absorption of water in bitumen.

Water diffusion in bitumen is dominated by water molecular states. The formation of hydrogen bonds and water clusters significantly decreases the water diffusion rate in bitumen. The diffusion coefficient of free water in dilute water–bitumen systems is ca. 4.7×10^{-12} m^2/s–1.4×10^{-11} m^2/s at 313 K. The diffusion coefficient of water in water clusters decreases with increasing cluster size and could be 1–2 orders of magnitude smaller than that of free water. Water molecules hydrogen-bonded to functional groups of bitumen can be assumed as completely immobile compared to bitumen.

The density, glass transition temperature, viscosity, and cohesive energy were computed. In most cases, all these parameters decrease with increasing water content of bitumen, which coincides with the formation of hydrogen bonds and water clusters. When adding water molecules to bitumen, existing bitumen–bitumen hydrogen bonds can be replaced by water–bitumen hydrogen bonds. At high water contents, large water droplets with sizes close to the number of water molecules in the simulation box are formed, which further hinders the interactions between bitumen components. As a result, the cohesion of bitumen is weakened. The presence of these water droplets also reduces the glass transition temperature and viscosity of water–bitumen systems.

CRediT authorship contribution statement

Lili Ma: Writing – review & editing, Writing – original draft, Software, Visualization, Investigation, Formal analysis, Data curation. **Hirad S. Salehi:** Writing – review & editing, Validation, Software, Data curation. **Ruxin Jing:** Data curation. **Sandra Erkens:** Funding acquisition. **Thijs J.H. Vlugt:** Writing – review & editing, Resources, Methodology. **Othonas A. Moultos:** Writing – review & editing, Writing – original draft, Supervision, Methodology, Investigation, Data curation, Conceptualization. **Michael L. Greenfield:** Writing – review & editing, Writing – original draft, Supervision, Software, Methodology, Investigation, Formal analysis, Conceptualization. **Aikaterini Varveri:** Writing – review & editing, Supervision, Funding acquisition, Conceptualization.

Declaration of competing interest

The authors declare the following financial interests/personal relationships which may be considered as potential competing interests: Lili Ma reports financial support was provided by China Scholarship Council. Aikaterini Varveri reports financial support was provided by Dutch Research Council. Othonas A. Moultos reports equipment, drugs, or supplies was provided by Dutch Research Council.

Data availability

Data will be made available on request.

Acknowledgments

This publication is part of the project ‘A multiscale approach towards future road infrastructure: How to design sustainable paving materials?’ (project number 18148) financed by the Dutch Research Council (NWO) Talent Programme Veni AES 2020. LM acknowledges support from the China Scholarship Council (CSC). This work was sponsored by NWO Domain Science for the use of supercomputer facilities. MLG acknowledges prior support from the US Fulbright Scholar program that initiated this collaboration. The authors acknowledge the use of computational resources of DelftBlue supercomputer, provided by Delft High Performance Computing Centre (https://www.tudelft.nl/dhpc).

Appendix A. Supplementary data

Supplementary material related to this article can be found online at https://doi.org/10.1016/j.conbuildmat.2023.133828.

References

[1] S. Rudyk, Relationships between SARA fractions of conventional oil, heavy oil, natural Bitumen and residues, Fuel 216 (2018) 330–340.
[2] J. Read, D. Whiteoak, Shell Bitumen Handbook, Thomas Telford, London, 2003.
[3] K. Kanitpong, H.U. Bahia, Role of adhesion and thin film tackiness of asphalt binders in moisture damage of HMA (with discussion), J. Assoc. Asphalt Pav. Technol. 72 (2003) 502–528.
[4] A. Diab, Z. You, Z. Hossain, M. Zaman, Moisture susceptibility evaluation of nanosize hydrated lime-modified asphalt–aggregate systems based on surface free energy concept, Transp. Res. Rec. 2446 (2014) 52–59.
[5] S. Caro, E. Masad, A. Bhasin, D.N. Little, Moisture susceptibility of asphalt mixtures, part 2: Characterisation and modelling, Int. J. Pav. Eng. 9 (2) (2008) 99–114.
[6] F. Canestrari, F. Cardone, A. Graziani, F.A. Santagata, H.U. Bahia, Adhesive and cohesive properties of asphalt-aggregate systems subjected to moisture damage, Road Mater. Pav. Des. 11 (sup1) (2010) 11–32.
[7] X. Wang, J. Ren, X. Gu, N. Li, Z. Tian, H. Chen, Investigation of the adhesive and cohesive properties of asphalt, mastic, and mortar in porous asphalt mixtures, Constr. Build. Mater. 276 (2021) 122255.
[8] D. Cheng, D.N. Little, R.L. Lytton, J.C. Holste, Moisture damage evaluation of asphalt mixtures by considering both moisture diffusion and repeated-load conditions, Transp. Res. Rec. 1832 (1) (2003) 42–49.
[9] R. Moraes, R. Velasquez, H.U. Bahia, Measuring the effect of moisture on asphalt–aggregate bond with the Bitumen bond strength test, Transp. Res. Rec. 2209 (1) (2011) 70–81.
[10] P. Chaturabong, H.U. Bahia, Effect of moisture on the cohesion of asphalt mastics and bonding with surface of aggregates, Road Mater. Pav. Des. 19 (3) (2018) 741–753.
[11] H.A. Omar, N.I.M. Yusoff, M. Mubaraki, H. Ceylan, Effects of moisture damage on asphalt mixtures, J. Traffic Transp. Eng. (English Ed.) 7 (5) (2020) 600–628.
[12] L. Ma, A. Varveri, R. Jing, S. Erkens, Comprehensive review on the transport and reaction of oxygen and moisture towards coupled oxidative ageing and moisture damage of Bitumen, Constr. Build. Mater. 283 (2021) 122632.
[13] R.L. Terrel, S. Al-Swailmi, Water Sensitivity of Asphalt-Aggregate Mixes: Test Selection, Tech. Rep. SHRP-A-403, Strategic Highway Research Program, National Research Council, Washington, D.C., 1994.
[14] M. Nobakht, D. Zhang, M.S. Sakhaeifar, R.L. Lytton, Characterization of the adhesive and cohesive moisture damage for asphalt concrete, Constr. Build. Mater. 247 (2020) 118616.
[15] J.C. Petersen, R.E. Robertson, J.F. Branthaver, P.M. Harnsberger, J.J. Duvall, S.S. Kim, D.A. Anderson, D.W. Christiansen, H.U. Bahia, Binder Characterization and Evaluation, Volume 1, Tech. Rep. SHRP-A-367, Strategic Highway Research Program, National Research Council, Washington, D.C., 1994.
[16] J.C. Petersen, A Review of the Fundamentals of Asphalt Oxidation: Chemical, Physicochemical, Physical Property, and Durability Relationships, Tech. Rep. E-C140, Transportation Research Board, Transportation Research Circular, Washington, DC, 2009.
[17] P.R. Herrington, J.P. Wu, L.C. van den Kerkhof, S.A. Bagshaw, Water diffusion in Bitumen films, Constr. Build. Mater. 294 (2021) 123530.
[18] L. Ma, A. Varveri, R. Jing, C. Kasbergen, S. Erkens, Thermodynamics and kinetics of moisture transport in Bitumen, Mater. Des. 222 (2022) 111028.
[19] Z. Cheng, F. Kong, X. Zhang, Application of the langmuir-type diffusion model to study moisture diffusion into asphalt films, Constr. Build. Mater. 268 (2021) 121192.
[20] A.K. Apeagyei, J.R.A. Grenfell, G.D. Airey, Evaluation of moisture sorption and diffusion characteristics of asphalt mastics using manual and automated gravimetric sorption techniques, J. Mater. Civ. Eng. 26 (2014) 04014045, http://dx.doi.org/10.1061/(ASCE)MT.1943-5533.0000929.
[21] K.L. Vasconcelos, A. Bhasin, D.N. Little, Measurement of water diffusion in asphalt binders using Fourier transform infrared–attenuated total reflectance, Transp. Res. Rec. 2179 (1) (2010) 29–38.
[22] A.K. Apeagyei, J.R. Grenfell, G.D. Airey, Application of Fickian and non-Fickian diffusion models to study moisture diffusion in asphalt mastics, Mater. Struct. 48 (5) (2015) 1461–1474.
[23] M. Chen, J. Geng, H. Chen, Y. Niu, R. Wang, W. Wu, S. Zhao, Z. Zhong, Diffusion of moisture and oxygen in Bitumens using electrochemical impedance spectroscopy, Fuel 315 (2022) 123212.
[24] A. Varveri, Moisture Damage Susceptibility of Asphalt Mixtures: Experimental Characterization and Modelling (Ph.D. thesis), Delft University of Technology, 2017.
[25] K.L. Vasconcelos, A. Bhasin, D.N. Little, History dependence of water diffusion in asphalt binders, Int. J. Pav. Eng. 12 (5) (2011) 497–506.
[26] T. Nguyen, W.E. Byrd, D. Bentz, J. Seiler Jr., Development of a Technique for In Situ Measurement of Water at the Asphalt/Model Siliceous Aggregate Interface, Tech. Rep. SHRP-ID/URF-92-611, Strategic Highway Research Program, 1992.
[27] D.D. Li, M.L. Greenfield, Chemical compositions of improved model asphalt systems for molecular simulations, Fuel 115 (2014) 347–356.
[28] C.A. Lemarchand, M.L. Greenfield, J.S. Hansen, Dynamics and structure of Bitumen–water mixtures, J. Phys. Chem. B 120 (24) (2016) 5470–5480.
[29] P.W. Jennings, J.A. Pribanic, M.A. Desando, M.F. Raub, F. Stewart, J. Hoberg, R. Moats, J.A. Smith, T.M. Mendes, M. McGrane, B. Fanconi, D.L. VanderHart, W.F. Manders, Binder Characterization and Evaluation by Nuclear Magnetic Resonance Spectroscopy, Tech. Rep. SHRP-A-335, Strategic Highway Research Program, National Research Council, Washington, D.C., 1993.
[30] M.L. Greenfield, Molecular modelling and simulation of asphaltenes and bituminous materials, Int. J. Pav. Eng. 12 (2011) 325–341.
[31] L. Zhang, M.L. Greenfield, Analyzing properties of model asphalts using molecular simulation, Energy Fuels 21 (3) (2007) 1712–1716.
[32] L. Zhang, M.L. Greenfield, Effects of polymer modification on properties and microstructure of model asphalt systems, Energy Fuels 22 (5) (2008) 3363–3375.
[33] J.S. Hansen, C.A. Lemarchand, E. Nielsen, J.C. Dyre, T. Schrøder, Four-component united-atom model of Bitumen, J. Chem. Phys. 138 (9) (2013) 094508.
[34] D.R. Jones, SHRP Materials Reference Library, Asphalt Cements: A Concise Data Compilation, Tech. Rep. SHRP-A-645, Strategic Highway Research Program, National Research Council, Washington, DC, 1993.
[35] S. Ren, X. Liu, P. Lin, Y. Gao, S. Erkens, Molecular dynamics simulation on bulk Bitumen systems and its potential connections to macroscale performance: Review and discussion, Fuel 328 (2022) 125382.
[36] G. Xu, H. Wang, Study of cohesion and adhesion properties of asphalt concrete with molecular dynamics simulation, Comput. Mater. Sci. 112 (2016) 161–169.
[37] Z. Liu, L. Cao, T. Zhou, Z. Dong, Multiscale investigation of moisture-induced structural evolution in asphalt–aggregate interfaces and analysis of the relevant chemical relationship using atomic force microscopy and molecular dynamics, Energy Fuels 34 (4) (2020) 4006–4016.
[38] Z. Du, X. Zhu, Y. Zhang, Diffusive dynamics and structural organization of moisture in asphaltic materials based on molecular dynamics simulation, J. Mater. Civ. Eng. 33 (1) (2021) 04020403.
[39] S. Ren, X. Liu, P. Lin, Y. Gao, S. Erkens, Review on the diffusive and interfacial performance of bituminous materials: From a perspective of molecular dynamics simulation, J. Mol. Liq. 366 (2022) 120363.
[40] S.H. Jamali, L. Wolff, T.M. Becker, M. De Groen, M. Ramdin, R. Hartkamp, A. Bardow, T.J.H. Vlugt, O.A. Moultos, OCTP: A tool for on-the-fly calculation of transport properties of fluids with the order-*n* algorithm in LAMMPS, J. Chem. Inform. Model. 59 (4) (2019) 1290–1294.
[41] F. Khabaz, R. Khare, Molecular simulations of asphalt rheology: Application of time–temperature superposition principle, J. Rheol. 62 (4) (2018) 941–954.
[42] W.L. Jorgensen, D.S. Maxwell, J. Tirado-Rives, Development and testing of the OPLS all-atom force field on conformational energetics and properties of organic liquids, J. Am. Chem. Soc. 118 (45) (1996) 11225–11236.
[43] G.A. Kaminski, R.A. Friesner, J. Tirado-Rives, W.L. Jorgensen, Evaluation and reparametrization of the OPLS-AA force field for proteins via comparison with accurate quantum chemical calculations on peptides, J. Phys. Chem. B 105 (28) (2001) 6474–6487.
[44] M.G. Martin, MCCCS Towhee: A tool for Monte Carlo molecular simulation, Mol. Simul. 39 (2013) 1212–1222.
[45] D.D. Li, M.L. Greenfield, High internal energies of proposed asphaltene structures, Energy Fuels 25 (2011) 3698–3705.
[46] W.M. Brown, A. Kohlmeyer, S.J. Plimpton, A.N. Tharrington, Implementing molecular dynamics on hybrid high performance computers–particle–particle particle-mesh, Comput. Phys. Comm. 183 (3) (2012) 449–459.
[47] H. Berendsen, J. Grigera, T. Straatsma, The missing term in effective pair potentials, J. Phys. Chem. 91 (24) (1987) 6269–6271.
[48] I.N. Tsimpanogiannis, O.A. Moultos, L.F. Franco, M.B.d.M. Spera, M. Erdős, I.G. Economou, Self-diffusion coefficient of bulk and confined water: A critical review of classical molecular simulation studies, Mol. Simul. 45 (4–5) (2019) 425–453.
[49] I.N. Tsimpanogiannis, S.H. Jamali, I.G. Economou, T.J.H. Vlugt, O.A. Moultos, On the validity of the Stokes–Einstein relation for various water force fields, Mol. Phys. 118 (9–10) (2020) e1702729.
[50] Y. Wu, H.L. Tepper, G.A. Voth, Flexible simple point-charge water model with improved liquid-state properties, J. Chem. Phys. 124 (2) (2006) 024503.
[51] P. Mark, L. Nilsson, Structure and dynamics of the TIP3P, SPC, and SPC/E water models at 298 K, J. Phys. Chem. A 105 (43) (2001) 9954–9960.
[52] H.C. Andersen, Rattle: A "velocity" version of the shake algorithm for molecular dynamics calculations, J. Comput. Phys. 52 (1) (1983) 24–34.
[53] J.-P. Ryckaert, G. Ciccotti, H.J. Berendsen, Numerical integration of the Cartesian equations of motion of a system with constraints: Molecular dynamics of *n*-alkanes, J. Comput. Phys. 23 (3) (1977) 327–341.
[54] T.W. Kennedy, G.A. Huber, E.T. Harrigan, R.J. Cominsky, C.S. Hughes, H. Von Quintus, J.S. Moulthrop, Superior Performing Asphalt Pavements (Superpave): The Product of the SHRP Asphalt Research Program, Tech. Rep. SHRP-A-410, Strategic Highway Research Program, 1994, Available on-line from http://www.trb.org/publications/shrp/SHRP-A-410.pdf.
[55] D.D. Li, M.L. Greenfield, Viscosity, relaxation time, and dynamics within a model asphalt of larger molecules, J. Chem. Phys. 140 (3) (2014) 034507.
[56] S. Plimpton, Fast parallel algorithms for short-range molecular dynamics, J. Comput. Phys. 117 (1) (1995) 1–19.

[57] A.P. Thompson, H.M. Aktulga, R. Berger, D.S. Bolintineanu, W.M. Brown, P.S. Crozier, P.J. in't Veld, A. Kohlmeyer, S.G. Moore, T.D. Nguyen, et al., LAMMPS - a flexible simulation tool for particle-based materials modeling at the atomic, meso, and continuum scales, Comput. Phys. Comm. 271 (2022) 108171.
[58] L. Martínez, R. Andrade, E.G. Birgin, J.M. Martínez, PACKMOL: A package for building initial configurations for molecular dynamics simulations, J. Comput. Chem. 30 (13) (2009) 2157–2164.
[59] M.P. Allen, D.J. Tildesley, Computer Simulation of Liquids, Oxford University Press, Oxford, 2017.
[60] F.W. Starr, J.K. Nielsen, H.E. Stanley, Hydrogen-bond dynamics for the extended simple point-charge model of water, Phys. Rev. E 62 (1) (2000) 579–587.
[61] E. Sevick, P. Monson, J. Ottino, Monte Carlo calculations of cluster statistics in continuum models of composite morphology, J. Chem. Phys. 88 (2) (1988) 1198–1206.
[62] S.H. Jamali, L. Wolff, T.M. Becker, A. Bardow, T.J.H. Vlugt, O.A. Moultos, Finite-size effects of binary mutual diffusion coefficients from molecular dynamics, J. Chem. Theory Comput. 14 (5) (2018) 2667–2677.
[63] O.A. Moultos, Y. Zhang, I.N. Tsimpanogiannis, I.G. Economou, E.J. Maginn, System-size corrections for self-diffusion coefficients calculated from molecular dynamics simulations: The case of CO_2, *n*-alkanes, and poly(ethylene glycol) dimethyl ethers, J. Chem. Phys. 145 (7) (2016) 074109.
[64] S.H. Jamali, R. Hartkamp, C. Bardas, J. Söhl, T.J.H. Vlugt, O.A. Moultos, Shear viscosity computed from the finite-size effects of self-diffusivity in equilibrium molecular dynamics, J. Chem. Theory Comput. 14 (11) (2018) 5959–5968.
[65] I.-C. Yeh, G. Hummer, System-size dependence of diffusion coefficients and viscosities from molecular dynamics simulations with periodic boundary conditions, J. Phys. Chem. B 108 (40) (2004) 15873–15879.
[66] A.T. Celebi, S.H. Jamali, A. Bardow, T.J.H. Vlugt, O.A. Moultos, Finite-size effects of diffusion coefficients computed from molecular dynamics: A review of what we have learned so far, Mol. Simul. 47 (10–11) (2021) 831–845.
[67] S.H. Jamali, A. Bardow, T.J.H. Vlugt, O.A. Moultos, Generalized form for finite-size corrections in mutual diffusion coefficients of multicomponent mixtures obtained from equilibrium molecular dynamics simulation, J. Chem. Theory Comput. 16 (6) (2020) 3799–3806.
[68] M.L. Greenfield, Simulation of small molecule diffusion using continuous space disordered networks, Mol. Phys. 102 (2004) 421–430.
[69] L. Luo, L. Chu, T. Fwa, Molecular dynamics analysis of oxidative aging effects on thermodynamic and interfacial bonding properties of asphalt mixtures, Constr. Build. Mater. 269 (2021) 121299.
[70] F. Khabaz, R. Khare, Glass transition and molecular mobility in styrene–butadiene rubber modified asphalt, J. Phys. Chem. B 119 (44) (2015) 14261–14269.
[71] J. Wang, R.M. Wolf, J.W. Caldwell, P.A. Kollman, D.A. Case, Development and testing of a general Amber force field, J. Comput. Chem. 25 (2004) 1157–1174.
[72] R.E. Robertson, J.F. Branthaver, P.M. Harnsberger, J.C. Peterson, S.M. Dorrence, J.F. McKay, T.F. Turner, A.T. Pauli, S.-C. Huang, J.-D. Huh, J.E. Tauer, K.P. Thomas, D.A. Netzel, F.P. Miknis, T. Williams, J.J. Duvall, F.A. Barbour, C. Wright, Fundamental Properties of Asphalts and Modified Asphalts, Volume 1; Interpretive Report. No. FHWA-RD-99-212, Tech. rep., United States. Federal Highway Administration, 2001.
[73] T.P. Turner, J.F. Branthaver, DSC studies of asphalts and asphalt components, in: A.M. Usmani (Ed.), Asphalt Science and Technology, Marcel Dekker, New York, 1997, pp. 59–101.
[74] C.A. Angell, K.L. Ngai, G.B. McKenna, P.F. McMillan, S.W. Martin, Relaxation in glassforming liquids and amorphous solids, J. Appl. Phys. 88 (6) (2000) 3113–3157.
[75] K. Oba, F. Björk, Dynamic mechanical properties of single-ply roof coverings for low-slope roofs and the influence of water, Polym. Test. 12 (1) (1993) 35–56.
[76] C.A. Lemarchand, N.P. Bailey, B.D. Todd, P.J. Daivis, J.S. Hansen, Non-Newtonian behavior and molecular structure of cooee Bitumen under shear flow: A non-equilibrium molecular dynamics study, J. Chem. Phys. 142 (24) (2015) 244501.
[77] A. Baldi-Sevilla, M.L. Montero, J.P. Aguiar-Moya, L.G. Loria-Salazar, A. Bhasin, Influence of Bitumen and aggregate polarity on interfacial adhesion, Road Mater. Pav. Des. 18 (sup2) (2017) 304–317.
[78] T. Nguyen, E.W. Byrd, D. Bentz, J. Martin, In situ spectroscopic study of water at the asphalt/siliceous substrate interface and its implication in stripping, J. Adhes. 81 (1) (2005) 1–28.